ENGINEERING TRANSACTIONS • *Engng. Trans.* • **62**, 2, 131–169, 2014
Polish Academy of Sciences • Institute of Fundamental Technological Research (IPPT PAN)
National Engineering School of Metz (ENIM) • Poznan University of Technology

Stresses and Displacements in an Elliptically Perforated Circular Disc Under Radial Pressure

Christos F. MARKIDES, Stavros K. KOURKOULIS

National Technical University of Athens
School of Applied Mathematical and Physical Sciences, Department of Mechanics
5 Heroes of Polytechnion Avenue, Theocaris Bld., Zografou Campus, 157 73 Athens, Greece
e-mail: stakkour@central.ntua.gr

The complex potentials governing the elastic equilibrium of a finite circular disc, elliptically perforated at its center, are obtained using Muskhelishvili's formulation. The disc is subjected to non-uniform distribution of pressure along two symmetric finite arcs of its periphery. Given the complex potentials, the stress- and displacement-fields can be determined everywhere on the disc by introducing a novel flexible interpretation of the conformal mapping, suitably adjusted to the computational process. The results of this procedure are given for various strategic loci and are critically discussed. The length of the loaded arc is considered similar to that obtained from the solution of the intact disc-circular jaw elastic contact problem assuming that the disc is compressed between the steel jaws of the device suggested by the International Society for Rock Mechanics for the implementation of the Brazilian-disc test. Concerning the distribution of the externally induced pressure along the loaded arcs, it is proven that for the general asymmetric configuration (i.e. the axes of the elliptical hole are neither parallel nor normal to the loading axis) the induced asymmetric displacement field does not permit maintenance of equilibrium of the disc as a whole in case the disc is considered exclusively under a distribution of radial pressure: Additional tractions must be exerted along the loaded arcs, obviously in the form of frictional stresses. Besides, providing full-field, analytic expressions for stresses and displacements, the main advantage of the present solution is that, by properly choosing the ratio of the ellipse's semi-axes, the solution of three additional configurations, of major importance in engineering praxis, are obtained: These of the intact disc, the circular ring and the cracked disc.

Key words: circular disc, ring, complex potentials, stress field, displacement field, fracture toughness, cracked Brazilian-disc test.

1. Introduction

The configuration of a circular disc of radius R_O and thickness w, either intact or centrally cracked, subjected to radial compressive loading along two finite arcs (symmetric with respect to the disc's center) of its periphery, is very familiar among scientists working experimentally for the indirect determination

of the tensile strength (intact disc) and the fracture toughness (cracked disc) of brittle geomaterials. Although both tests are long ago standardized [1–3], quite a few issues are still to be confronted, especially for the case of the cracked configuration [4, 5]. These issues are mainly related to the lack of convincing closed-form solutions for the corresponding stress- and displacement-fields, which is in turn responsible for the adoption of approximate (and quite often erroneous) formulae for the respective Stress Intensity Factors (SIFs).

It is to be accepted from the very beginning that the specific problem, i.e. to obtain accurate closed formulae for stresses and displacements for a cracked body of finite dimensions, is very complicated, even in its simplest form, i.e. for discs made of elastic, homogenous and fully isotropic materials. The accurate simulation of the actual boundary conditions (distribution of radial pressure, length of the loaded arcs) [6], the mutual contact of the crack lips (for specific crack inclinations with respect to the loading axis) [7–9] and the rotation of the crack axis during loading [9–11] are perhaps the main reasons for the difficulties encountered when one is seeking for a reliable general solution of the problem.

Existing solutions are restricted to discs with a central mathematical crack (an ideal cut of zero distance between its lips) of length 2α, loaded by a pair of forces P linearly distributed along two generatrices of the disc (symmetric with respect to the disc's center) (Fig. 1a). The pioneering work of Atkinson *et al.* [12] is perhaps the most representative and widely adopted approach of this class. Recently, the problem was re-solved by considering a finite circular disc with a relatively "short" central crack of mathematical nature assuming that the external force P/w is uniformly distributed (Fig. 1b) along two arcs of finite length equal to $2\omega_o R_O$ [13]. In other words, the disc was assumed to be loaded by uniform radial pressure $\sigma_r = P/(2R_O\omega_o w)$. It was shown that as

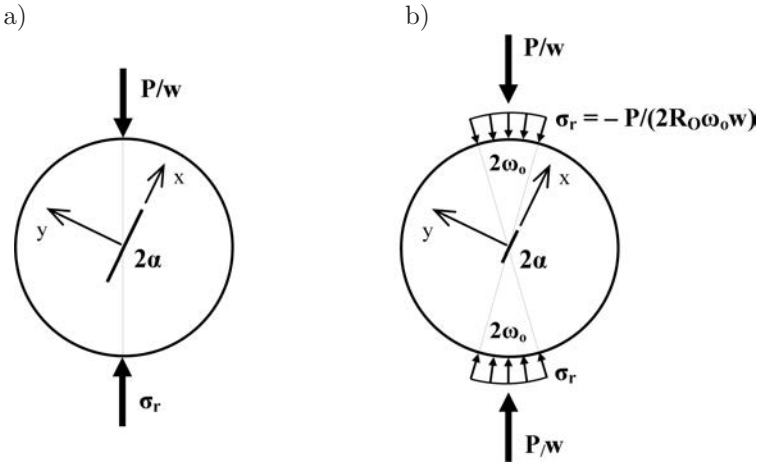

Fig. 1. The circular disc under point forces (a) and uniform radial pressure (b).

long as the length of the crack does not exceed one fourth of the disc's radius, the solution obtained was very close to that proposed by Atkinson *et al.* [12] for point forces. In both cases, however, it was clearly indicated that for crack inclinations (with respect to the loading axis) exceeding a certain limit (around 30°) the crack lips are coming into mutual contact rendering the formulae for stresses and displacements erroneous [12, 13].

In an effort to overcome the as above mentioned complexities, an alternative approach is here proposed by considering a finite circular disc with a central elliptical cut instead of either a mathematical crack [12, 13] or of a rectangular slit (a cut of constant distance between its lips) [14]. In addition, instead of adopting either uniform pressure [13] or point forces [12], a more realistic loading scheme is adopted. This scheme is based on the parabolic distribution of radial pressure obtained from the solution of the respective contact problem for the intact disc [15]. As long as the solution is obtained for an arbitrary elliptical hole, it is then straightforward to arrive to the solution of a cracked disc (by letting the minor semi-axis of the ellipse approach zero), or to the solution of a circular ring (by letting the minor semi-axis of the ellipse approach the major one) or even to the solution of the intact disc (by assuming that the lengths of the semi-axes tend to zero). In this way, the whole range of configurations (i.e. from the solid disc to the circular ring and to the cracked disc) is covered.

In the present study attention is paid to the solution of the mathematical problem (and the procedure followed to arrive at analytic expressions for the stresses and displacements) as well as to the way the respective formulae are to be applied (in conjunction with an alternative interpretation of the conformal mapping) rather than to the practical aspects and applications of the formula obtained.

The solution for the elliptically perforated disc is considered in juxtaposition to the ones for the circular ring and the intact disc and interesting comparative conclusions are drawn concerning the respective stress fields. Moreover, interesting conclusions are drawn concerning the role of the boundary conditions and especially for the kind of the distribution of the external loading. Interestingly enough, it is shown that the equilibrium of the elliptically perforated disc cannot be ensured (assuming that the crack is neither normal nor parallel to the loading axis) by considering exclusively radial pressure along the loaded rims (as in the case of the intact disc or the ring): Additional tractions (perhaps in the form of shear/friction stresses) are required along the loaded arcs of the disc's periphery.

In addition, the deformed shape of the disc and the elliptic cut is thoroughly studied indicating that the axis of the ellipse is deformed obtaining a 'sigmoid' shape while on the other hand its lips are coming to partial contact either close to their tips or at their central region, depending on both the ratio of the semi-axes and the magnitude of the load.

2. Theoretical preliminaries

2.1. Formulation of the mathematical problem

An elliptically perforated disc of radius R_O and thickness w is squeezed by a force P_{frame} between the curved jaws of the device suggested by the International Society for Rock Mechanics (ISRM) [1] for the implementation, according to standardized manner, of the Brazilian-disc test (Fig. 2a). It is assumed that the disc is at a state of global equilibrium (i.e. no rigid-body rotation is allowed). Under the above assumptions the stress- and displacement-fields developed all over the disc's area are to be determined.

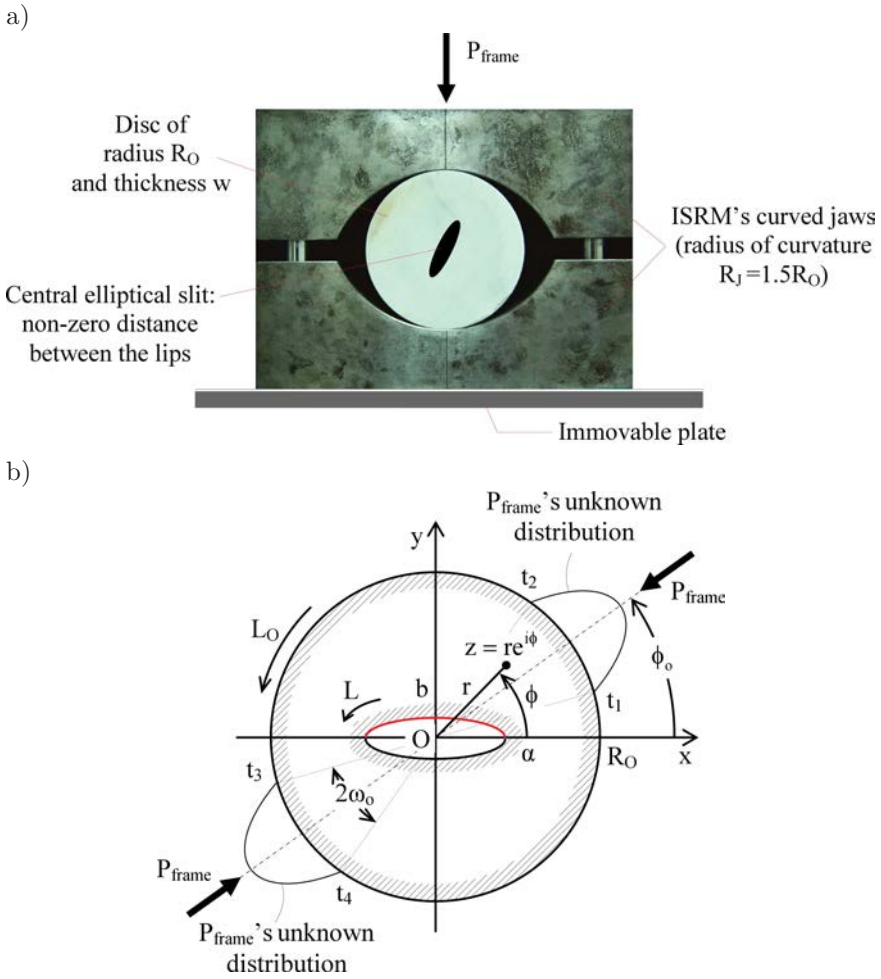

Fig. 2. a) Elliptically perforated disc compressed between the jaws of the ISRM device for the standardized implementation of the Brazilian-disc test, b) the configuration of the mathematical problem.

Considering the problem as a plane one, the configuration of the isolated disc is shown in Fig. 2b: An elliptically perforated circular disc of radius R_O with a stress-free central elliptical hole L is lying in the $z = x + iy = re^{i\phi}$ complex plane. The origin of the Cartesian reference is the centre of the disc. Denote by α and b the major and minor axes of L, respectively. The major axis α of L is aligned along x-axis. The external loading, P_{frame}, forms an angle ϕ_o with respect to α. P_{frame}/w is distributed along two symmetric arcs t_1t_2 and t_3t_4 of the disc's periphery L_O, each one equal to $2R_O\omega_o$. For the time being the nature of the distribution of P_{frame} on the disc's cross section is considered unknown.

Assuming that the disc's material is homogeneous, isotropic and linearly elastic, Kolosov's [17] and Muskhelishvili's [18] complex potentials method is employed. For the solution to be achieved advantage is taken of the complex potentials characterizing the elastic equilibrium of a circular ring compressed between the jaws of the ISRM's suggested device for the implementation of the Brazilian-disc test. This solution was recently obtained [19] and it is very briefly recapitulated in Subsec. 2.2.

It is mentioned, however, that following an alternative approach, one could equally well take advantage of the respective intact disc's solution [20]. The ring's solution was chosen in the present study just because it was proven more convenient for the particular case since it has been obtained in series form [19]: It is therefore relieved from logarithmic terms (appearing in the intact disc's solution) which in turn render the procedure for obtaining the principal parts of analytic functions (involved during the solution) much more complicated.

2.2. The complex potentials for the circular ring under parabolic pressure [19]

A circular ring of the same dimensions as the elliptically perforated disc (thickness w, outer radius R_O) is considered with an inner hole of radius R_I. Its cross-section lies at the $z = x + iy = re^{i\phi}$ complex plane and the origin of the Cartesian reference is taken at its centre. The ring is assumed to be subjected to a parabolic pressure $\sigma_r = -P(\phi)$ (statically equivalent to the overall load P_{frame}) along two symmetric arcs of its outer periphery L_O, each one of length $2R_O\omega_o$. The axis of symmetry of the externally induced load forms an angle ϕ_o, measured in the counter clockwise direction from x-axis (Fig. 3). Both $P(\phi)$ and ω_o are assumed to be given by the respective contact problem through the expressions [15, 16]:

$$\omega_o = \text{Arcsin}\sqrt{\frac{6KP_{\text{frame}}}{\pi R_O w}} \qquad \text{and} \qquad P(\phi) = P_c\left[1 - \frac{\sin^2(\phi_o - \phi)}{\sin^2\omega_o}\right], \tag{2.1}$$

where

$$K = \frac{\kappa + 1}{4\mu} + \frac{\kappa_J + 1}{4\mu_J} \qquad \text{and} \qquad P_c = P(\phi)_{\max} = \sqrt{\frac{3\pi P_{\text{frame}}}{32KR_O w}}. \tag{2.2}$$

In Eqs. (2.1) and (2.2) P_c is the maximum value of $P(\phi)$ attained at $\phi = \phi_o$. In addition, κ, κ_J and μ, μ_J are Muskhelishvili's [18] constants (which are equal to $(3-4\nu)$ for plane strain and $(3-\nu)/(1+\nu)$ for plane stress, with ν denoting the Poisson's ratio) and shear moduli of the disc's and jaw's materials, respectively.

Alternatively, one can arbitrarily prescribe angle ω_o and thus avoid resorting to the contact problem. In this case, instead of using Eq. $(2.2)_2$, parameter P_c should be defined as:

$$P_c = P(\phi)_{\max} = \frac{2P_{\text{frame}} \sin^2 \omega_o}{R_O w \left(\sin 2\omega_o - 2\omega_o \cos 2\omega_o\right)}. \tag{2.3}$$

According to Ref. [19], the complex potentials characterizing the ring's equilibrium are:

$$\phi_o(z) = \frac{P_c}{\pi}\left\{ b_0 z + \frac{B_2}{3} z^3 - B_{-2} z^{-1} + \sum_{n=1}^{\infty}\left[\frac{B_{4n}}{4n+1} z^{4n+1} - \frac{B_{-4n}}{4n-1} z^{-(4n-1)} + \frac{B_{2(2n+1)}}{4n+3} z^{4n+3} - \frac{B_{-2(2n+1)}}{4n+1} z^{-(4n+1)} \right] \right\}, \tag{2.4}$$

$$\psi_o(z) = \frac{P_c}{\pi}\left\{ B'_0 z + \frac{B'_2}{3} z^3 - b'_{-2} z^{-1} - \frac{B'_{-4}}{3} z^{-3} + \sum_{n=1}^{\infty}\left[\frac{B'_{4n}}{4n+1} z^{4n+1} + \frac{B'_{2(2n+1)}}{4n+3} z^{4n+3} - \frac{B'_{-4(n+1)}}{4n+3} z^{-(4n+3)} - \frac{B'_{-2(2n+1)}}{4n+1} z^{-(4n+1)} \right] \right\}. \tag{2.5}$$

The complex constants B_j, B'_j, which appear in Eqs. (2.4) and (2.5), are straightforwardly obtained from the respective constants b_j, b'_j, which were determined in Ref. [19], by simply rotating the co-ordinate system adopted in Ref. [19] through a positive angle $(\pi/2 - \phi_o)$. For brevity, the explicit expressions of these constants are given in Appendix A.

3. The stress- and displacement-fields in an elliptically perforated disc

3.1. The complex potentials

For the transition from the ring's configuration to that of the elliptically perforated disc to be achieved, consider an ellipse L of major axis α and minor axis b (where α is aligned along x-axis) at the center of the ring of Fig. 3, as it is shown in Fig. 4a. By properly removing parts from the ring and/or adding patches of the very same material to it (see the dashed areas in Fig. 4a), the

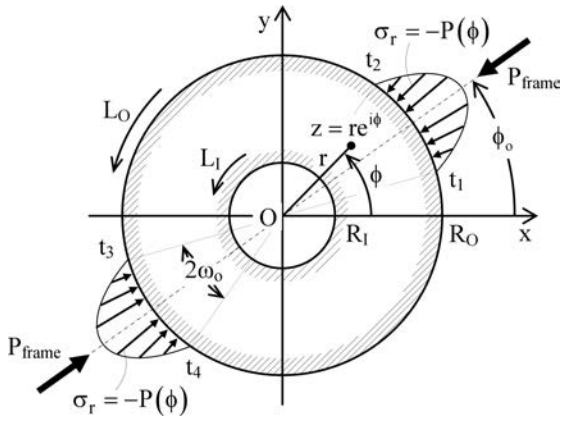

FIG. 3. The circular ring under parabolically distributed pressure.

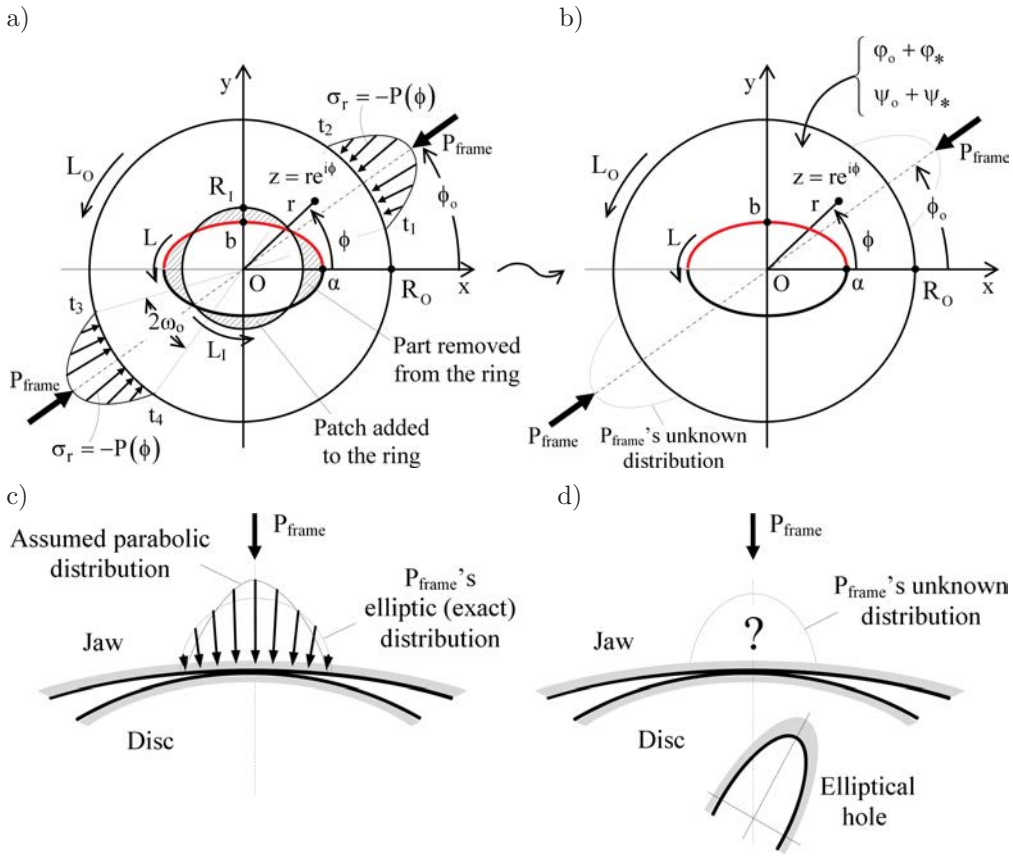

FIG. 4. a) The transition from the ring to the elliptically perforated disc, b) the elliptically perforated disc under an overall external force P_{frame}, c) the solution of the elastic intact disc-jaw contact problem and d) the implication due to the asymmetric configuration of the elliptically perforated disc.

configuration of the elliptically perforated disc is obtained. In this case, the solution of the elliptically perforated disc is sought in the following form:

$$\begin{aligned} \varphi(z) &= \varphi_o(z) + \varphi_*(z), \\ \psi(z) &= \psi_o(z) + \psi_*(z), \end{aligned} \tag{3.1}$$

where $\varphi_o(z)$, $\psi_o(z)$ represent the solution of the circular ring (Eqs. (2.4) and (2.5)) while $\varphi_*(z)$ and $\psi_*(z)$ are additional analytic functions, due to the presence of the elliptical hole, which are to be determined.

The configuration of the elliptically perforated disc is shown in Fig. 4b. In this figure, the set of functions of Eqs. (3.1) shown are to emphatically stress that the nature of the distribution of P_{frame} along the loaded arc is not a-priori known whereas it is known that the state of elastic equilibrium is governed by these functions. In other words, the parabolic distribution of radial pressure obtained in Ref. [15] refers to the case of two **symmetric** semi-infinite circular bodies (the disc and the jaw of the ISRM device) which come in smooth mutual contact (Fig. 4c). Obviously, this is definitely not the case for the **asymmetric** problem solved here, since the disc contains an elliptical hole the dimensions of which are well comparable to the disc's radius (Fig. 4d).

From the theoretical point of view, the transition from the ring to the elliptically perforated disc is realized according to the following two-steps procedure:

i. Firstly, the region of the ring outside L is conformally mapped onto the region outside the unit hole γ (Fig. 5) in the mathematical $\zeta = \xi + i\eta = \rho e^{i\theta}$ complex plane ($s = e^{i\theta}$ denotes the point ζ on γ) through the function:

$$z = \omega(\zeta) = R(\zeta + m/\zeta). \tag{3.2}$$

In Eq. (3.2) parameters R and m are defined as $R = (\alpha + b)/2$ and $m = (\alpha - b)/(\alpha + b)$. In accordance with this transformation, Eqs. (3.1) are re-written as:

$$\begin{aligned} \varphi(\zeta) &= \phi_o(\zeta) + \varphi_*(\zeta), \\ \psi(\zeta) &= \psi_o(\zeta) + \psi_*(\zeta), \end{aligned} \tag{3.3}$$

ii. As a second step the boundary L is demanded to be free from stresses. In other words, the following boundary condition is imposed [18]:

$$\varphi(s) + \frac{s^2 + m}{s(1 - ms^2)}\overline{\varphi'(s)} + \overline{\psi(s)} = 0. \tag{3.4}$$

In Eq. (3.4) over-bar denotes the complex conjugate while prime indicates first order derivative.

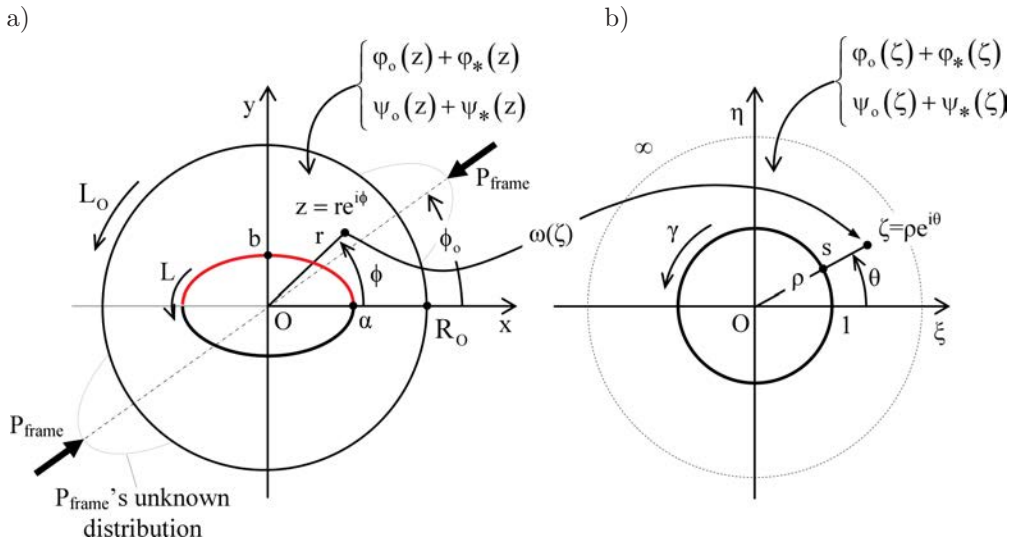

FIG. 5. The conformal mapping of the elliptically perforated disc (a) to the unit circle (b).

Introducing Eqs. (3.3) into Eq. (3.4) one arrives at the following equation for the functions $\varphi_*(\zeta)$ and $\psi_*(\zeta)$ which were to be determined:

$$\varphi_*(s)+\frac{s^2+m}{s(1-ms^2)}\overline{\varphi_*'(s)}+\overline{\psi_*(s)} = \underbrace{-\left[\varphi_o(s)+\frac{s^2+m}{s(1-ms^2)}\overline{\varphi_o'(s)}+\overline{\psi_o(s)}\right]}_{f_*(s)}. \tag{3.5}$$

At this point L_O is considered as if it were lying at infinity and φ_* and ψ_* were vanishing there. In such a case MUSKHELISHVILI'S [18] formulae for the infinite plate provide these functions as:

$$\begin{aligned}\varphi_*(\zeta) &= -\frac{1}{2\pi i}\int_\gamma \frac{f_*(s)\,ds}{s-\zeta},\\ \psi_*(\zeta) &= -\frac{1}{2\pi i}\int_\gamma \frac{\overline{f_*(s)}\,ds}{s-\zeta}-\zeta\frac{1+m\zeta^2}{\zeta^2-m}\phi_*'(\zeta).\end{aligned} \tag{3.6}$$

Combining now Eqs. (2.4), (2.5), (3.2), (3.5), (3.6) one obtains the functions $\varphi_*(\zeta)$ and $\psi_*(\zeta)$. Then by taking advantage of Eqs. (3.3) the functions $\varphi(\zeta)$ and $\psi(\zeta)$ are determined as follows:

$$\varphi(\zeta)=\frac{P_cR}{\pi}\Bigg\{\left(b_0+mR^2B_2\right)\zeta+\frac{R^2B_2}{3}\zeta^3 - \frac{mb_0+\overline{B_0'}+R^2\left[\left(1+2m^2\right)\overline{B_2}+m\overline{B_2'}\right]}{\zeta}-\left(m\overline{B_2}+\frac{\overline{B_2'}}{3}\right)\frac{R^2}{\zeta^3} + \sum_{n=1}^{\infty}R^{4n}\Bigg[\frac{B_{4n}}{4n+1}G_{4n+1}^{\infty}(\zeta)-\overline{B_{4n}}G_{4n}^{0}(\zeta)-\frac{\overline{B_{4n}'}}{4n+1}G_{4n+1}^{0}(\zeta) + R^2\left(\frac{B_{2(2n+1)}}{4n+3}G_{4n+3}^{\infty}(\zeta)-\overline{B_{2(2n+1)}}G_{2(2n+1)}^{0}(\zeta)-\frac{\overline{B_{2(2n+1)}'}}{4n+3}G_{4n+3}^{0}(\zeta)\right)\Bigg]\Bigg\}, \tag{3.7}$$

$$\psi(\zeta)=\frac{P_cR}{\pi}\frac{\zeta^2}{\zeta^2-m}\Bigg\{\left(B_0'+\frac{2mR^2B_2'}{3}\right)\zeta+\frac{R^2B_2'}{3}\zeta^3 - \left(\frac{8m\overline{B_2}}{3}+\overline{B_2'}\right)\frac{R^2}{\zeta^5}-\frac{R^2\left(4\frac{1+3m^2}{3}\overline{B_2}+2m\overline{B_2'}\right)+\overline{B_0'}}{\zeta^3} - 2\frac{\left(1+m^2\right)\left(b_0+2mR^2\Re B_2\right)+m\Re\left(B_0'+mR^2B_2'\right)}{\zeta} + \left(\frac{1}{\zeta}+m\zeta\right)\sum_{n=1}^{\infty}R^{4n}\Bigg[\overline{B_{4n}}\frac{dG_{4n}^{0}(\zeta)}{d\zeta}-\frac{B_{4n}}{4n+1}\frac{dG_{4n+1}^{\infty}(\zeta)}{d\zeta}+\frac{\overline{B_{4n}'}}{4n+1}\frac{dG_{4n+1}^{0}(\zeta)}{d\zeta} + R^2\left(\overline{B_{2(2n+1)}}\frac{dG_{2(2n+1)}^{0}(\zeta)}{d\zeta}-\frac{B_{2(2n+1)}}{4n+3}\frac{dG_{4n+3}^{\infty}(\zeta)}{d\zeta}+\frac{\overline{B_{2(2n+1)}'}}{4n+3}\frac{dG_{4n+3}^{0}(\zeta)}{d\zeta}\right)\Bigg] - \left(1-\frac{m}{\zeta^2}\right)\sum_{n=1}^{\infty}R^{4n}\Bigg[\frac{\overline{B_{4n}}}{4n+1}G_{4n+1}^{0}(\zeta)-B_{4n}G_{4n}^{\infty}(\zeta)-\frac{B_{4n}'}{4n+1}G_{4n+1}^{\infty}(\zeta) + R^2\left(\frac{\overline{B_{2(2n+1)}}}{4n+3}G_{4n+3}^{0}(\zeta)-B_{2(2n+1)}G_{2(2n+1)}^{\infty}(\zeta)-\frac{B_{2(2n+1)}'}{4n+3}G_{4n+3}^{\infty}(\zeta)\right)\Bigg]\Bigg\}. \tag{3.8}$$

In the above formulae $\Re$ denotes the real part. Furthermore, $G_j^{\infty}(\zeta)$ and $G_j^{0}(\zeta)$ are the principal parts of analytic functions involved at the point at infinity and at $\zeta=0$, respectively. Their analytic expressions are given (in the order they appear) for brevity in Appendix B. In the same Appendix B, the way one should deal with Cauchy type integrals during the derivation of $\varphi_*(\zeta)$ as well as the way one can obtain $G_{4n+1}^{\infty}(\zeta)$ are shown as an illustration.

It is to be emphasized at this point that, although, for example

$$\lim_{R_O \to \infty} (B_{4n}) = 0$$

(recall that the $R_O \to \infty$ assumption has been adopted for the Muskhelishvili's formulae for infinite domains to be applied), B_{4n} is assumed to maintain a finite constant value keeping in mind that, due to the bounded character of the region considered here, infinity is never reached. Similar conclusions are drawn for the remaining constants B_j, B'_j.

Obviously, by letting $R_O \to \infty$, both φ_* and ψ_* tend to zero on L_O and the solution of the elliptically perforated disc turns to coincide with that of the ring on the disc's periphery. Clearly, in this particular case the distribution of P_{frame} along the loaded arc comprises exclusively radial pressure described by the second of Eqs. (2.1).

3.2. Some mathematical hints

It is observed from Eqs. (3.7) and (3.8) that the complex potentials φ and ψ, standing for the solution of the elliptically perforated disc, are given in terms of the $\zeta = \rho e^{i\theta}$ variable (i.e. in the mathematical plane) instead of reverting to the variable $z = re^{i\phi}$ on the real disc. The inversion of the transformation is then implemented according to an alternative approach, i.e. by using the modulus ρ and the argument θ of variable ζ. This alternative is found to be very convenient in the computational process when deriving certain numerical results while the respective formulae are kept rather short. Indeed, taking advantage of the $\zeta = \left(z + \sqrt{z^2 - 4mR^2}\right)/(2R)$ relation (obtained by solving Eq. (3.2) for ζ), ρ and θ, are directly determined in terms of the corresponding modulus and argument r and ϕ of z as follows:

$$\rho(r,\phi) = \frac{1}{2R}\left[r^2 + \sqrt{r^4 + 16m^2R^4 - 8mr^2R^2\cos 2\phi} \right.$$
$$+2r \cdot \sqrt[4]{r^4 + 16m^2R^4 - 8mr^2R^2\cos 2\phi}$$
$$\left. \cdot \cos\left(\phi - \frac{1}{2}\arctan\frac{r^2\sin 2\phi}{r^2\cos 2\phi - 4mR^2}\right)\right]^{1/2} \tag{3.9}$$

$$\theta(r,\phi) = \arctan\frac{r\sin\phi + \sqrt[4]{r^4 + 16m^2R^4 - 8mr^2R^2\cos 2\phi}\cdot a^*}{r\cos\phi + \sqrt[4]{r^4 + 16m^2R^4 - 8mr^2R^2\cos 2\phi}\cdot b^*},$$

where

$$a^* = \sin\left(\frac{1}{2}\arctan\frac{r^2\sin 2\phi}{r^2\cos 2\phi - 4mR^2}\right),$$

$$b^* = \cos\left(\frac{1}{2}\arctan\frac{r^2\sin 2\phi}{r^2\cos 2\phi - 4mR^2}\right).$$

In the above formulae it holds that $0 \le \phi < 2\pi$ and $r_{L,\phi} \le r \le R_O$, where

$$r_{L,\phi} = \sqrt{\left\{\alpha\cos\left[\operatorname{Arc\,tan}\left(\frac{\alpha}{b}\tan\phi\right)\right]\right\}^2 + \left\{b\sin\left[\operatorname{Arc\,tan}\left(\frac{\alpha}{b}\tan\phi\right)\right]\right\}^2} \tag{3.10}$$

is the radius of the elliptical hole for the particular angle ϕ. In fact, it can be proven that Eqs. (3.9) are the parametric equations of:

i. A class of curves called '*hippopedes*'.

ii. A class of curves which are orthogonal to the above '*hippopedes*', in the ζ-plane.

In this way, instead of adopting the usual representation of the transformation (which corresponds ellipses and hyperbolas of the z-plane (Fig. 6a) to circles and radii in the ζ-plane (Fig. 6b)), an alternative and more representative interpretation of the transformation is chosen here, which corresponds the circles and radii (making up the real disc in the z-plane) (Fig. 6c) to '*hippopedes*' and orthogonal curves in the ζ-plane (Fig. 6d).

It is emphasized at this point that utmost attention should be paid when dealing with the multi-valued arctan$(*)$ functions, appearing in the expressions for ρ and θ (Eqs. (3.9)), in order for continuity to be maintained. In this direction, a multi-coloured auxiliary sketch is shown in Fig. 6d indicating the various intervals of r and ϕ at which proper values should be ascribed to the variation of the above arctan$(*)$ functions to avoid possible uncertainties when applying the respective formulae.

3.3. The stress field

The polar components of the stress field on the real disc in terms of the variable ζ in the mathematical plane are given by the well-known formulae [18]:

$$\begin{aligned} \sigma_\rho - i\sigma_{\rho\theta} &= 2\Re\Phi(\zeta) - \frac{\zeta^2}{\rho^2\overline{\omega'(\zeta)}}\left[\overline{\omega(\zeta)}\,\Phi'(\zeta) + \omega'(\zeta)\Psi(\zeta)\right], \\ \sigma_\rho + \sigma_\theta &= 4\Re\Phi(\zeta), \end{aligned} \tag{3.11}$$

where

$$\Phi(\zeta) = \frac{\varphi'(\zeta)}{\omega'(\zeta)}, \qquad \Psi(\zeta) = \frac{\psi'(\zeta)}{\omega'(\zeta)}. \tag{3.12}$$

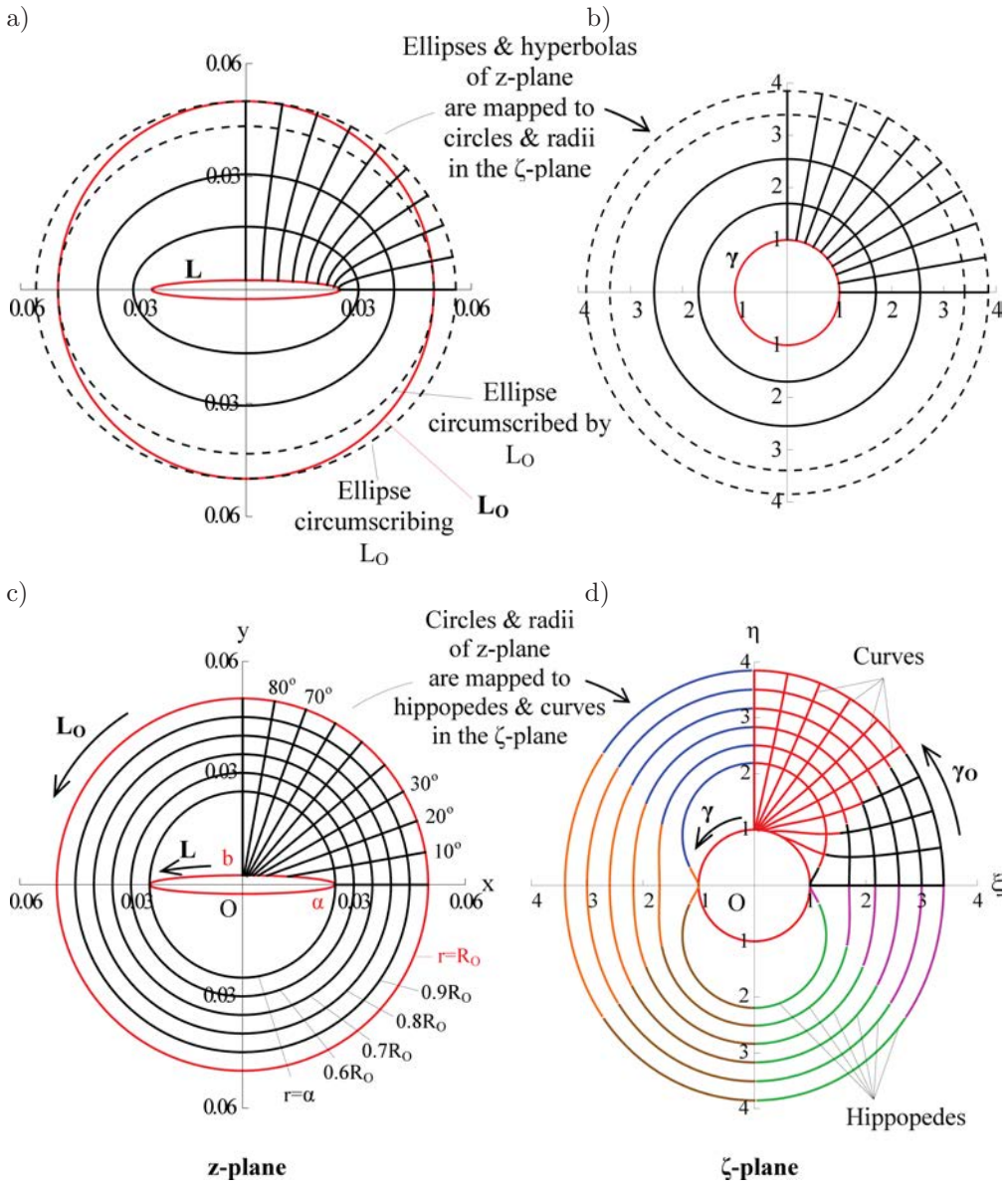

FIG. 6. Details of the mathematical analysis: Ellipses and hyperbolas of the z-plane (a) mapped to circles and radii in the ζ-plane (b). Circles and radii of the z-plane (c) mapped to "*hippopedes*" and curves normal to the "*hippopedes*" in the ζ-plane (d).

By combining Eqs. (3.2), (3.7), (3.8), (3.11), (3.12) the stresses are obtained everywhere on the disc.

In particular, the explicit formulae along x-axis (aligned along the major axis α of the elliptical hole), which is a locus of particular importance, are

given in Appendix C. It is emphasized that in these formulae, the variable quantity is the arbitrary point on ξ-axis in the mathematical ζ-plane which corresponds to the arbitrary point along x-axis on the real disc in the z-plane through the relation $\xi = (x + \sqrt{x^2 - 4mR^2})/(2R)$. For instance, for ξ in the $\left[1, \left(R_O + \sqrt{R_O^2 - 4mR^2}\right)/(2R)\right]$ interval one obtains the stresses along the positive x-axis in the $[\alpha, R_O]$ interval. Symbol $\Im$ in Eq. (C.2) of Appendix C denotes the imaginary part of a complex quantity.

As a characteristic example, the stress-field components (reduced over the amplitude of the parabolic pressure P_c) within the $\alpha \leq x \leq R_O$ interval are plotted in Fig. 7, according to the formulae of Appendix C. For the plots to be implemented, a disc with $R_O = 0.05$ m, $w = 0.01$ m, $\alpha = 0.5R_O$, $b = 0.2\alpha$ is considered. The disc is made of PMMA (elastic modulus $E = 3.19$ GPa and Poisson's ratio $\nu = 0.36$). The perforated disc is squeezed between the ISRM's curved jaws [1] (radius of curvature $R_J = 1.5R_O$), which are made of steel (elastic modulus $E_J = 210$ GPa and Poisson's ratio $\nu_J = 0.3$). An overall load $P_{\text{frame}} = 20$ kN is exerted on the upper jaw at an angle $\phi_o = 60°$ with respect to the major axis of the elliptical hole (Fig. 7). Plane strain conditions were assumed. For the specific case the solution of the respective contact problem for the intact disc (first of Eqs. (2.1)) provides a contact angle $2\omega_o = 23.75°$.

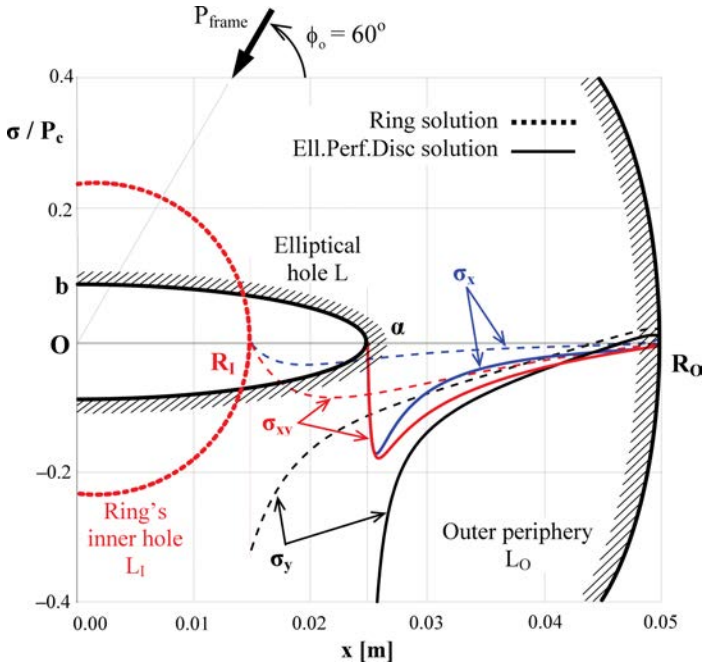

FIG. 7. The stress field components along the positive x-axis for the elliptically perforated disc (continuous line) and the circular ring (discontinuous line) plotted in juxtaposition for $\phi_o = 60°$.

For comparison reasons, the respective stress-field components for a ring [19], of the same dimensions and of the same material, with an inner hole L_I of radius $R_I = 0.3R_O$ are also shown in the same Fig. 7. For both solutions, a number of $n = 20$ additional terms in the respective infinite series solutions was considered.

The quantitative similarity between the graphs of the respective components for the two configurations is clear revealing that, though based on the infinite plate assumption, the solution of the elliptically perforated disc introduced provides very satisfactory results even in case the dimensions of the elliptical hole are well comparable to the disc's diameter. It is interesting to observe, however, that some differences are detected on the outer periphery L_O of the elliptically perforated disc, ascribed to the asymmetry of the specific configuration against the perfectly symmetric configuration of the problem of the circular ring. This point indicates that the boundary conditions of the elliptically perforated disc diversify from those of the ring (as it had to be expected) as a result of its inherent asymmetry and the rotation tendency inevitably induced on the disc by this asymmetry. Due to its crucial importance, the specific issue will be discussed thoroughly in Sec. 4.

3.4. The displacement field

Introducing Eqs. (3.2), (3.7), (3.8) into Muskhelishvili's well-known formula [18]

$$2\mu(u+iv) = \kappa\varphi(\zeta) - \frac{\omega(\zeta)}{\overline{\omega'(\zeta)}}\overline{\varphi'(\zeta)} - \overline{\psi(\zeta)} \tag{3.13}$$

the Cartesian components of the displacement-field components are obtained at any point of the disc. Due to their length, the explicit formulae are given in Appendix D. In these formulae both the horizontal and vertical components of the displacement field have been divided into two terms: These that are equal and these that are opposite at complex conjugate points on the disc so that $u = u_{\text{eq}} + u_{\text{op}}$ and $v = v_{\text{eq}} + v_{\text{op}}$. Such a partition is very convenient especially when dealing with the displacements of the elliptical hole L.

Next, some examples are given for some characteristic cases revealing vividly the nature of deformation. In these examples, for comparison reasons, three different configurations are considered in juxtaposition to each other:

i. An intact circular disc [21],
ii. A circular ring [19] and
iii. An elliptically perforated disc.

In all three cases discs with $R_O = 0.05$ m, $w = 0.01$ m and $\alpha = 0.5R_O$ are considered made of PMMA ($E = 3.19$ GPa, $\nu = 0.36$) and pressed against the

ISRM's steel ($E_J = 210$ GPa, $\nu_J = 0.3$) jaws. In particular, in Fig. 8a it is assumed that $b \to 0$, i.e. the elliptically perforated disc tends to the cracked disc. Moreover, for the ring configuration it is assumed that $R_{\rm I} = 0.1R_O$. In addition, for the displacements to be clearly distinguished in the plots, a relatively high external force $P_{\rm frame} = 140$ kN was exerted on the discs at a direction parallel to the major axis of the elliptic hole (i.e. it is assumed that $\phi_o = 0°$). Such a value for the external load seems perhaps unrealistic from a practical point of view, however it is well accepted from the theoretical point of view, since all three solutions compared are based on the linear elasticity assumption. Plain strain conditions were assumed for all three configurations.

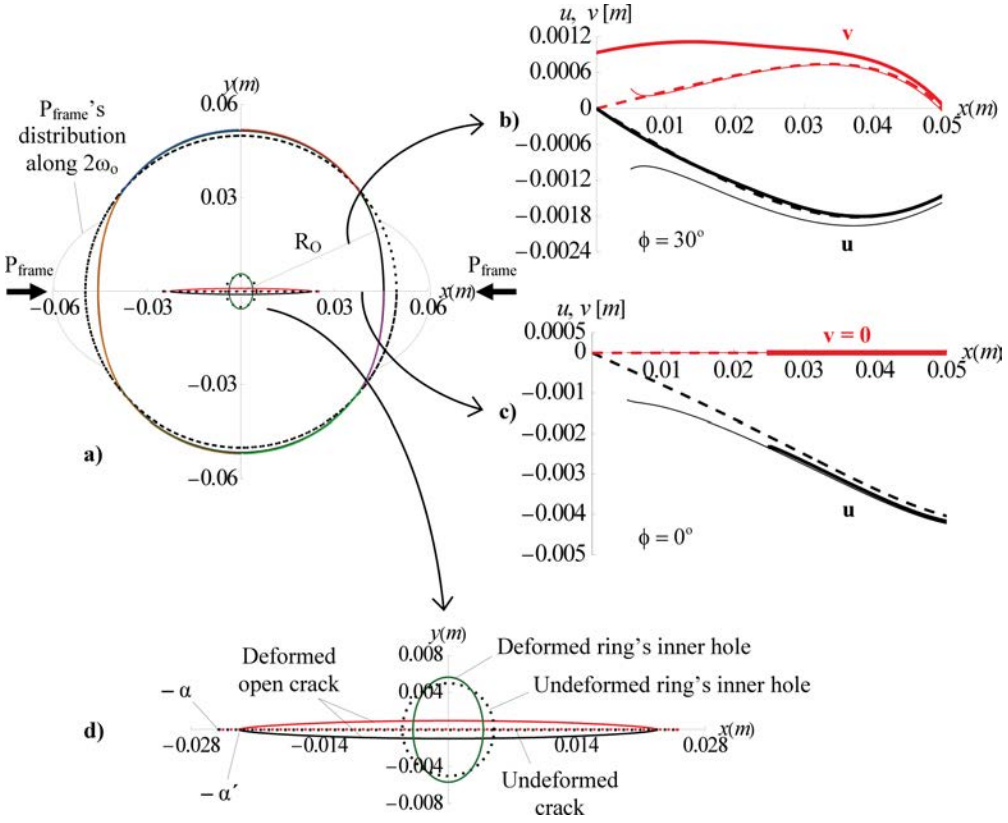

FIG. 8. Initial and deformed configurations of the intact disc, the circular ring and the elliptically perforated disc for $\phi_o = 0°$ (a). The displacement-field components for $\phi = 30°$ (b) and $\phi = 0°$ (c). Enlarged view of the central region of the ring and the elliptically perforated disc for $\phi_o = 0°$ (d).

For the as above set of numerical values, a contact angle $2\omega_o = 65.98°$ is obtained from the solution of the intact disc's contact problem. A number of

$n = 4$ additional terms in the ring's and elliptically perforated disc's solutions was considered.

The undeformed state is indicated by dotted lines. The deformed outer periphery is marked by black continuous line for the solid disc, green continuous line for the ring and multi-coloured (in accordance with Fig. 6d) line for the elliptically perforated disc. It is seen that it is difficult even to distinguish the deformed outer periphery of the three different configurations studied, a result supporting further the validity of the solution introduced. In Figs. 8(b,c) the variation of the Cartesian components of the displacement along the radius with $\phi = 30^\circ$ and along x-axis ($\phi = 0^\circ$) respectively, are shown, again for all three geometries studied. Discontinuous lines correspond to the solid disc, thin continuous lines to the ring whereas thick continuous lines correspond to the elliptically perforated disc. Finally, in Fig. 8d, an enlarged view of the central

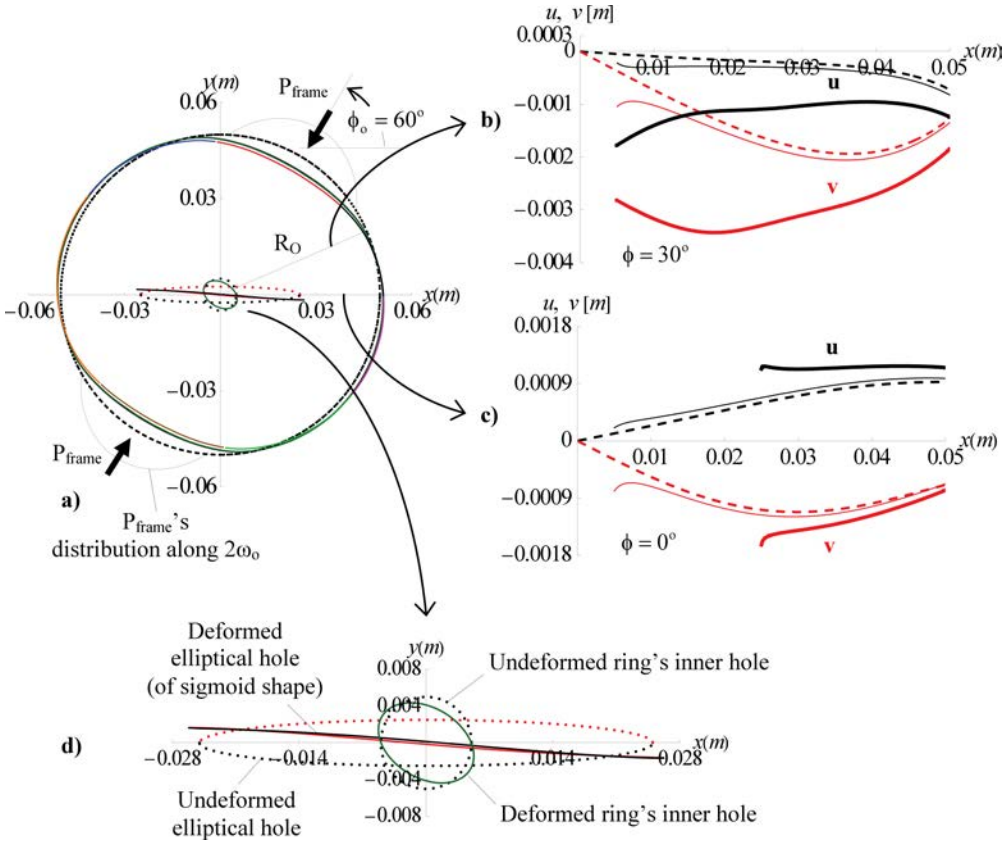

FIG. 9. Initial and deformed configurations of the intact disc, the circular ring and the elliptically perforated disc for $\phi_o = 60^\circ$ (a). The displacement-field components for $\phi = 30^\circ$ (b) and $\phi = 0^\circ$ (c). Enlarged view of the central region of the ring and the elliptically perforated disc for $\phi_o = 60^\circ$ (d).

region of all three configurations is presented: The expected symmetric opening of the crack (red colour indicates the upper lip) as well as the symmetric distortion (transformation to an elliptical hole) of the ring's inner circular hole (green colour) are clearly seen. In addition, it is observed that the crack tip, α, is displaced inwards (towards the centre of the disc) at a new point α' of x-axis.

In order now to demonstrate the crucial role of the load axis direction, the geometry with $\phi_o = 60^\circ$ is studied for the same as previously set of numerical data. The only difference is that now the minor axis of the elliptical hole b instead of tending to zero is assumed equal to 0.1α. The results are presented in Fig. 9, along the same line of thought as they were plotted in Fig. 8. It is seen that from a qualitative point of view the results are more or less similar to those of Fig. 8. The crucial (and critical) difference is that now an unnatural overlapping of the lips of the elliptical hole is detected (Fig. 9d). Such an unnatural phenomenon was long ago observed by Pazis *et al.* [9] for an infinite plate under biaxial loading conditions. What is worthy to be mentioned, however, is that contrary

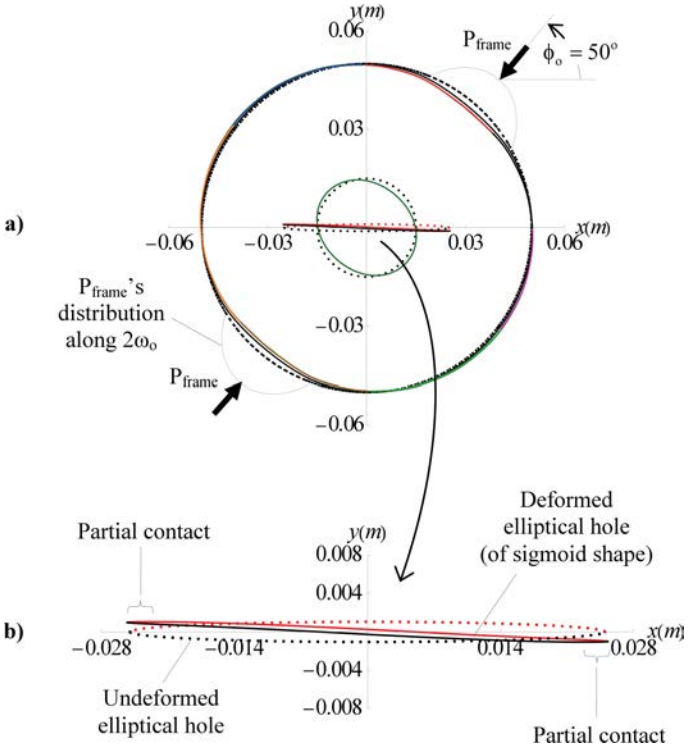

Fig. 10. Initial and deformed configurations of the intact disc, the circular ring and the elliptically perforated disc with a narrow hole for $\phi_o = 50^\circ$ (a). Enlarged view of the central region of the ring and the elliptically perforated disc for $\phi_o = 50^\circ$. Partial contact is realized around the tips of the elliptical hole (b).

to the case of the infinite plate, for which the deformed elliptical hole (either with open or overlapped lips) is still an ellipse, in the present case the deformed elliptical hole is transformed to a sigmoid shape showing vividly the crucial influence of the boundaries' finiteness on the deformation of the elliptical hole.

The width of the elliptical hole (i.e. the magnitude of b) in conjunction with the magnitude of the externally imposed load are crucial also for the nature of the deformation of the elliptical hole. For the same as previously set of numerical data a narrow ellipse is now considered with $b = 0.042\alpha$. In addition, an arbitrary value for the inner ring's hole $R_{\mathrm{I}} = 0.3R_O$ is considered. Moreover, a lower value of the external load $P_{\mathrm{frame}} = 50$ kN is imposed resulting to a contact angle $2\omega_o = 37.98°$. The inclination of the loading axis with respect to the axis of the ellipse is now $\phi_o = 50°$. The deformed geometries of all three configurations under study are plotted in Fig. 10. In the enlarged image of their central region (Fig. 10b) it

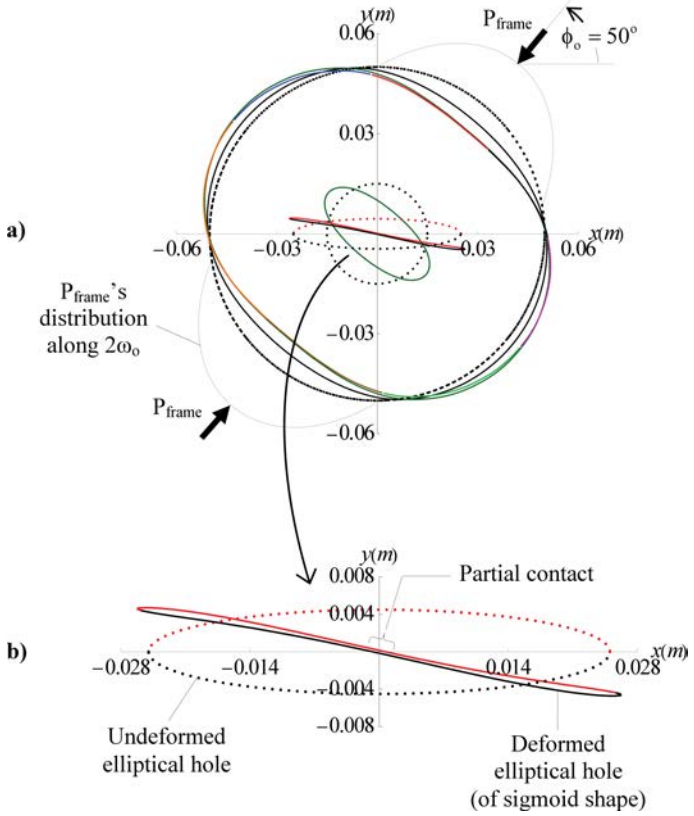

FIG. 11. Initial and deformed configurations of the intact disc, the circular ring and the elliptically perforated disc with a wide hole for $\phi_o = 50°$ (a). Enlarged view of the central region of the ring and the elliptically perforated disc for $\phi_o = 50°$. Partial contact is realized around the central portion of the elliptical hole (b).

is seen now that a partial contact is realized near the tips of the hole. Obviously, the contact length increases gradually towards the centre of the ellipse as the load increases further. It is very interesting to note that the above order is reversed in case the minor semi-axis of the elliptical hole increases: Contact appears initially at the central portion of the ellipse (expanding gradually towards the tips of the ellipse as the load increases). This is clearly seen in Fig. 11 where the same configurations with those of Fig. 10 are considered, but now the minor axis b of the elliptical hole attains a higher value equal to 0.18α while the load P_{frame} imposed is equal to 220 kN.

4. Discussion

Among the most controversial topics related to the practical applications of the configurations considered in the present work (cracked disc, circular ring, intact disc, and elliptically perforated disc) is to definitely (and accurately) describe the boundary conditions along the contact arcs.

While in existing contributions, both early [22] and relatively recent [20], the load has been assumed as uniformly distributed along a "small" contact arc of arbitrary length, indications existed (dated back to Timoshenko around 1910 [23]) that the load is distributed according to a much more complicated law. Particularly, in case of perfect symmetry (intact circular disc or ring with a relatively small inner hole), and in the absence of friction, the exact law describing the radial pressure at any arbitrary point τ of the contact arc is [15, 18, 23]:

$$P(\tau) = \frac{1}{3R_O K}\sqrt{\ell^2 - \tau^2},$$

where R_O is the radius of the disc, K is given by Eq. $(2.2)_1$ and $2\ell \approx 2R_O\omega_o$ is the length of the contact arc.

It is evident that in case the configuration ceases being symmetric (cracked disc, disc with elliptical hole) while the domains considered are still of finite dimensions, the as above distribution will be somehow distorted. The analytic character of the present solution offers in that case the means for quantifying this quite reasonable distortion (this has already been done, implicitly, in Subsec. 3.3 and 3.4, when comparing the boundary values of stresses and displacements on L_O due to the solution of the elliptically perforated disc in conjunction to the respective ones due to the ring's and the intact disc's configurations).

In this context one should begin from the general solution $\varphi = \varphi_o + \varphi_*$, $\psi = \psi_o + \psi_*$ of the elliptically perforated disc (recall, that this solution has been obtained by assuming that if L_O were lying infinity, φ_*, ψ_* would vanish there). Let now this region be transformed into the finite circular ring (Fig. 12a). It can be easily shown that the solution of the elliptically perforated disc, though based

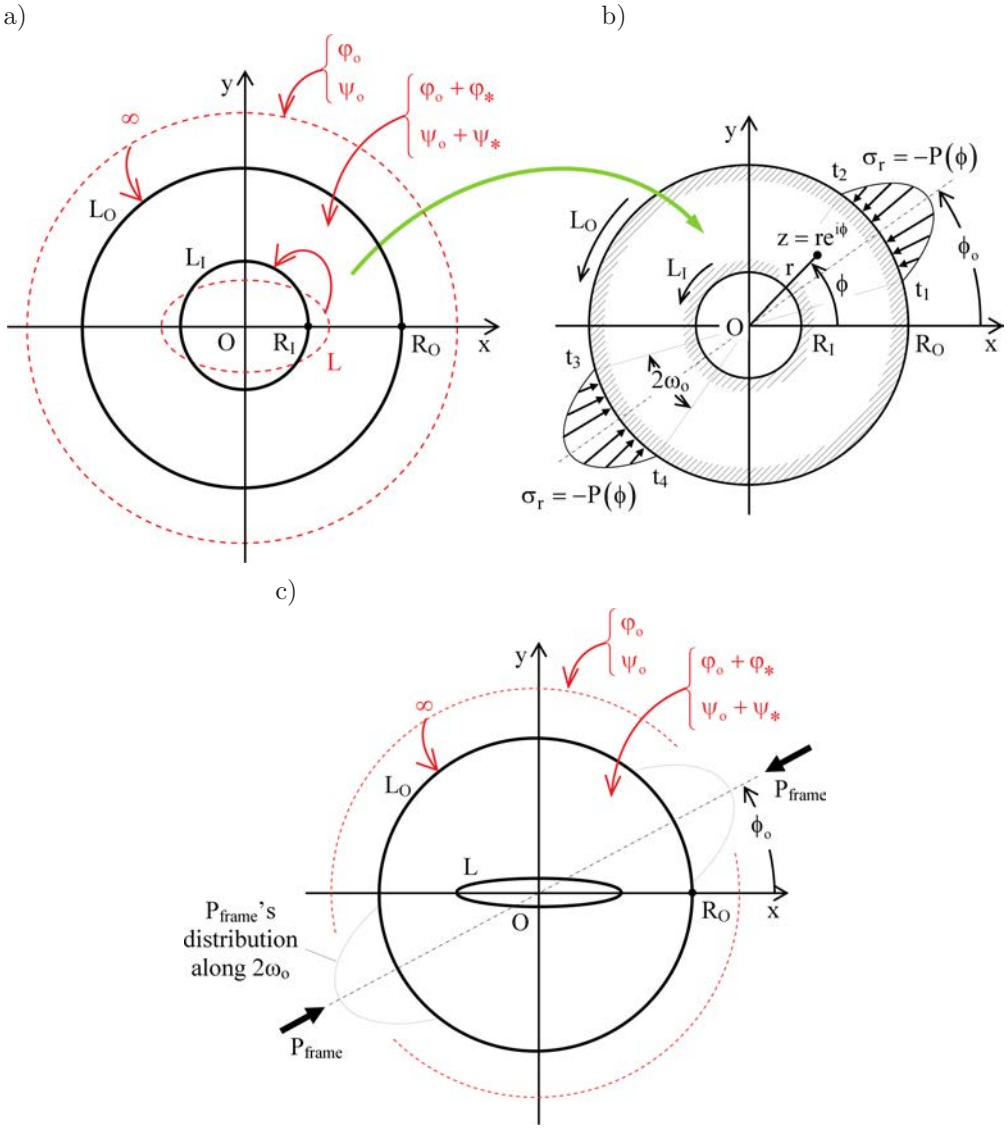

FIG. 12. Quantifying the inevitable distortion of the stress field due to the inherent geometric asymmetry of the configuration considered: Transformation of the elliptically perforated disc (a) to the ring (b) and the case of the elliptically perforated disc with a relatively big elliptical hole (c).

on the infinite plate formulae, provides with a unique accuracy the solution (for both stresses and displacements) of the finite ring under parabolic pressure [19] (Fig. 12b). It is thus seen that in this symmetric case the solution of the elliptically perforated disc provides sound boundary conditions along the loaded arc, indicating that indeed a single parabolic pressure does ensure global equilibrium

of the region considered. This fact, apart from being an additional evidence for the validity of the solution introduced here, implies also a conceivable connection between the solution of an infinite region and a finite one, at least in the case of configurations symmetric regarding both geometry and loading.

As a second step, the general asymmetric case is considered, i.e. that of the finite, elliptically perforated disc under an external loading forming an arbitrary angle ϕ_o with its major axis. Notice that in this case the present solution anticipates, by assumption, that when L_O lies at infinity or, what is equivalent, when the hole is very small, the influence of the latter on the former vanishes so that again a single parabolic pressure along the contact arc ensures global equilibrium describing, again, adequately the boundary conditions.

As a last step, let the dimensions of the elliptical hole be well comparable to the disc's radius so that φ_*, ψ_* will appear also in the solution of the problem near the outer periphery L_O (Fig. 12c). For such a configuration, the polar stresses along L_O of the elliptically perforated disc are plotted in Fig. 13a, for $R_O = 0.05$ m, $w = 0.01$ m, $\alpha = 0.5R_O$, $b = 0.1\alpha$, $P_{\text{frame}} = 50$ kN at $\phi_o = 30^\circ$ and plane strain conditions, resulting to a contact angle $2\omega_o = 37.98^\circ$. The number n of additional terms taken into account was equal to 50. Notice that these boundary stresses (the radial and the shear ones) are plotted out of a scale in Fig. 13b together with the undeformed (discontinuous line) and the deformed (continuous line) configurations of the elliptically perforated disc. As it is seen from these figures, a parabolic pressure alone acting along the loaded rims is not sufficient to maintain the global equilibrium of the disc contrary to the case when L_O lies at infinity, or equivalently when the elliptical hole is very small compared to the disc's radius. As L_O "comes" from infinity, or in other words as α becomes bigger and bigger, the influence of the crack on the outer periphery (and vice versa) is getting more and more intensive. As it is clearly seen, even the radial pressure along the contact arc is not exactly parabolic anymore; there is a slight but clear asymmetry in its variation: Notice for instance the difference between the altitudes of σ_r at the end points t_j of the loaded arcs in Fig. 13a.

What is more (and apart from some convergence issues involved in solutions given in infinite series form), it is seen that additional normal and shear stresses are required all along L_O to suffice the global equilibrium of the disc. Although their magnitude is small, compared to the radial pressure, they can by no means be ignored. This observation is in excellent agreement with the results of a recent study on the centrally cracked circular disc [10, 11]. In that study it was shown, that in the most general case (i.e. the external load is inclined with respect to the crack axis by an angle ϕ_o different from 0° or 90°) then, due to the rotation of the crack, the disc tends to rotate as a rigid body unless additional tangential frictional stresses are imposed along the loaded arcs (apart from the distribution of radial pressure).

a)

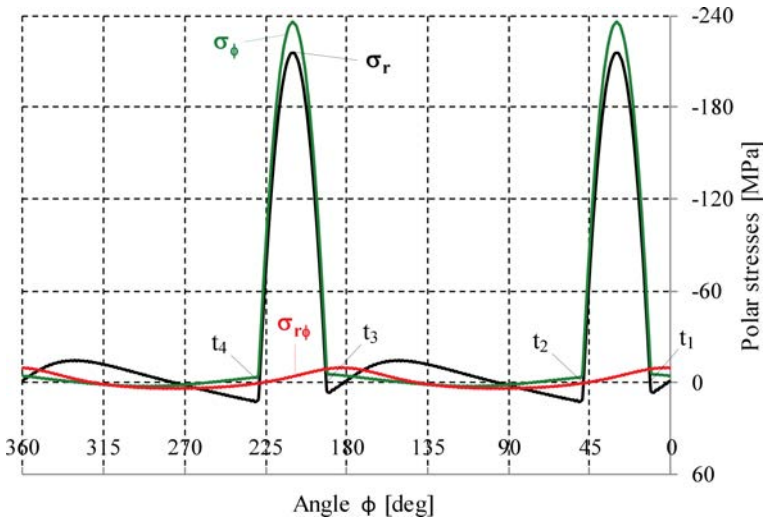

b)

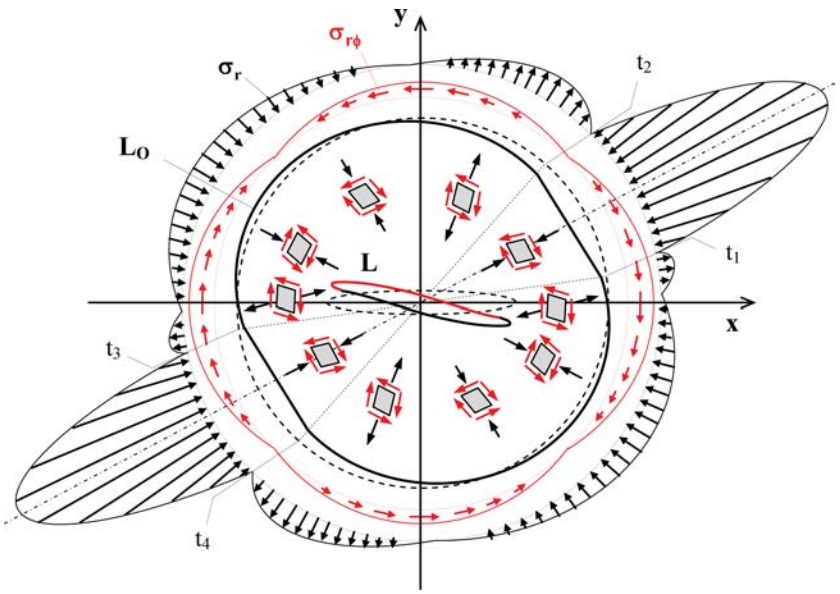

FIG. 13. The polar distribution of stresses along the periphery L_O of the elliptically perforated disc (a) and the boundary stresses (radial and shear), plotted out of a scale, together with the undeformed (discontinuous line) and deformed (continuous line) configurations of the elliptically perforated disc (b).

All this evidence supports the conclusion that for the solution for the elliptically perforated disc (as well as that for the cracked disc) to be meaningful a mere radial pressure is not enough and additional stresses are required along the contact arc.

Fortunately, for the particular case of full symmetry, i.e. for $\phi_o = 0°$, which is the most interesting one for the engineering community (recall that it provides experimentally the value of fracture toughness, K_{IC}), the infinite plate assumption is accurate (in the strict mathematical sense) for the finite elliptically perforated disc: A parabolic distribution of radial pressure alone ensures global equilibrium of the disc (Fig. 14a). This is evident also from Fig. 14b, in which the stresses along x-axis in the elliptically perforated disc and in the

a)

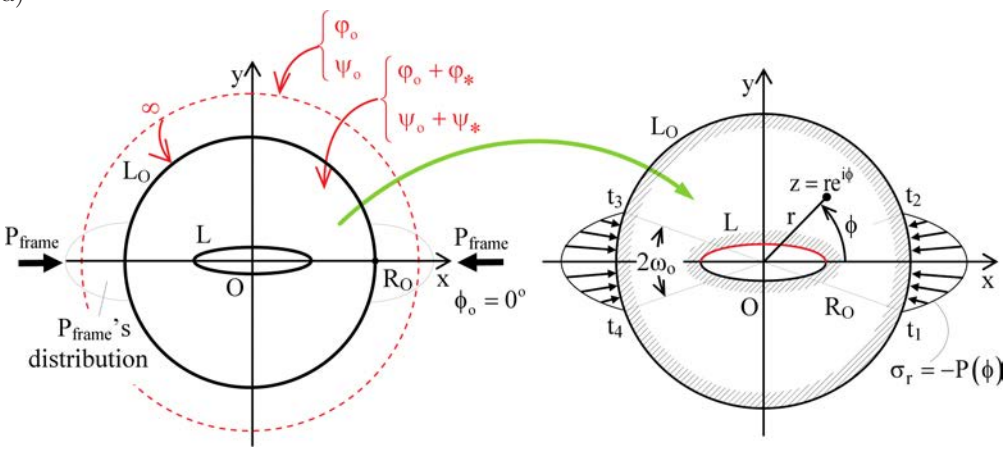

b)

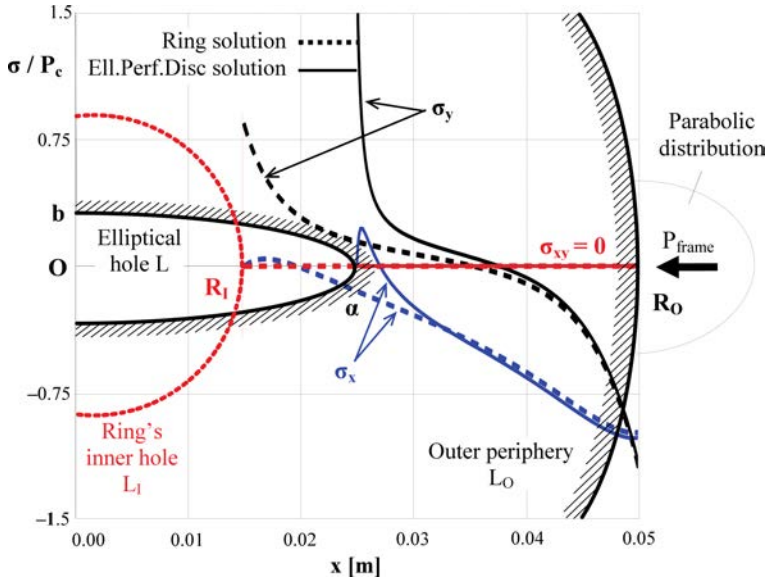

FIG. 14. The case of complete geometric symmetry ($\phi_o = 0°$) (a). The stress field components along the positive x-axis for the elliptically perforated disc (continuous line) and the circular ring (discontinuous line) plotted in juxtaposition for $\phi_o = 0°$.

circular ring are plotted in juxtaposition to each other (for the same data used in Subsec. 3.3 for $\phi_o = 0°$). Therefore, it is reasonable to conclude that the values of the Stress Intensity Factor which can be determined using the present solution (by moving along the x-axis towards the elliptical crack's tip) are very close to the exact ones and can be safely used in praxis for the determination of Fracture Toughness.

5. Conclusions

An analytic procedure was proposed providing full-field, closed expressions for the stress- and displacement-fields in an elliptically perforated disc under distributed loads along two finite arcs of its periphery. The main advantage of the procedure introduced is that by proper choice of the α/b ratio (i.e. the ratio of the major-over-minor semi-axes of the ellipse) one obtains the solution for a series of configurations widely used in engineering praxis. More specifically considering that α, $b \to 0$ one obtains the respective stress- and displacement fields for an intact disc, i.e. for the familiar Brazilian-disc test. By considering $b \to \alpha \neq 0$, the solution for the circular ring is obtained, i.e. for the familiar ring test. Finally, by assuming that $\alpha \neq 0$ and $b \to 0$ one arrives at the solution for the cracked circular disc which corresponds to the widely used test for the determination of Fracture Toughness of brittle materials.

The solution introduced is based on the adoption of more realistic description of the boundary conditions prevailing along the disc-jaw interface. These conditions approach closer the actual ones in case the disc is compressed between the jaws of the ISRM device for the standardized Brazilian-disc test. Therefore, there is no need for one to resort to arbitrary assumptions about the contact length and the kind of the distribution of the external load. Moreover, the formulae introduced are full-field, providing stresses and displacements everywhere on the disc and not only along some specific loci. Finally, the expressions obtained are of closed form and they are relatively easily programmable eliminating the need to resort to tabulated values.

The study revealed a potential connection between infinite and finite regions which has to be further investigated. Moreover, it was shown that the general asymmetric configuration of the problem leads to asymmetric deformation. It was thus definitely indicated that additional stresses are required along the loaded arcs, apart from a radial pressure distribution, for global equilibrium to be maintained. The latter is in complete agreement with the conclusions of an on-going research project concerning the rotation tendency of a cracked disc. It would be very interesting as a next step, to correlate the as above mentioned additional stresses with the frictional ones required to maintain global equilibrium and complete the problem of the circular disc with the elliptical hole

or the crack by accurately describing the complete set of boundary conditions as well as their influence on its periphery.

Appendix A. The coefficients of the series expansions of Eqs. (2.4), (2.5).

$$b_0 = \left(\frac{2\omega_o - \sin 2\omega_o}{4\sin^2 \omega_o} - \omega_o \right) \frac{R_O^2}{R_O^2 - R_I^2},$$

$$B_2 = \left(\frac{\omega_o - \sin 2\omega_o}{2\sin^2 \omega_o} + \frac{\sin 2\omega_o \cos 2\omega_o}{4\sin^2 \omega_o} + \sin 2\omega_o \right)$$
$$\cdot \frac{3\left(R_O^2 - R_I^2\right) - R_O^4\left(R_O^{-2} - R_I^{-2}\right)}{3\left(R_O^2 - R_I^2\right)^2 + \left(R_O^6 - R_I^6\right)\left(R_O^{-2} - R_I^{-2}\right)} \left(\cos 2\phi_o - i \sin 2\phi_o\right),$$

$$B_{-2} = \left(\frac{\omega_o - \sin 2\omega_o}{2\sin^2 \omega_o} + \frac{\sin 2\omega_o \cos 2\omega_o}{4\sin^2 \omega_o} + \sin 2\omega_o \right)$$
$$\cdot \frac{R_O^4\left(R_I^2 - R_O^2\right) + \left(R_I^6 - R_O^6\right)}{3\left(R_O^2 - R_I^2\right)^2 + \left(R_O^6 - R_I^6\right)\left(R_O^{-2} - R_I^{-2}\right)} \left(\cos 2\phi_o + i \sin 2\phi_o\right),$$

$$B_{4n} = \left(\frac{\sin 4n\omega_o}{4n\sin^2 \omega_o} + \frac{\sin 2\omega_o \cos 4n\omega_o - 2n\cos 2\omega_o \sin 4n\omega_o}{2\left(4n^2 - 1\right)\sin^2 \omega_o} - \frac{\sin 4n\omega_o}{2n} \right)$$
$$\cdot \frac{(1+4n)\left(R_O^2 - R_I^2\right) R_O^{-2(2n-1)} - \left[R_O^{-2(4n-1)} - R_I^{-2(4n-1)}\right] R_O^{2(2n+1)}}{(1-16n^2)\left(R_O^2 - R_I^2\right)^2 - \left[R_O^{2(4n+1)} - R_I^{2(4n+1)}\right]\left[R_O^{-2(4n-1)} - R_I^{-2(4n-1)}\right]}$$
$$\cdot \left(\cos 4n\phi_o - i \sin 4n\phi_o\right),$$

$$B_{-4n} = \left(\frac{\sin 4n\omega_o}{4n\sin^2 \omega_o} + \frac{\sin 2\omega_o \cos 4n\omega_o - 2n\cos 2\omega_o \sin 4n\omega_o}{2\left(4n^2 - 1\right)\sin^2 \omega_o} - \frac{\sin 4n\omega_o}{2n} \right)$$
$$\cdot \frac{(1-4n)\left(R_O^2 - R_I^2\right) R_O^{2(2n+1)} - \left[R_O^{2(4n+1)} - R_I^{2(4n+1)}\right] R_O^{-2(2n-1)}}{(1-16n^2)\left(R_O^2 - R_I^2\right)^2 - \left[R_O^{2(4n+1)} - R_I^{2(4n+1)}\right]\left[R_O^{-2(4n-1)} - R_I^{-2(4n-1)}\right]}$$
$$\cdot \left(\cos 4n\phi_o + i \sin 4n\phi_o\right),$$

$$B_{2(2n+1)} = \left[\frac{\sin 2\,(2n+1)\,\omega_o}{2\,(2n+1)\sin^2\omega_o} + \frac{\sin 2\omega_o \cos 2\,(2n+1)\,\omega_o - (2n+1)\cos 2\omega_o \sin 2\,(2n+1)\,\omega_o}{8n\,(n+1)\sin^2\omega_o} - \frac{\sin 2\,(2n+1)\,\omega_o}{2n+1} \right]$$

$$\cdot \frac{(4n+3)\left(R_O^2 - R_I^2\right) R_O^{-4n} - \left[R_O^{-2(4n+1)} - R_I^{-2(4n+1)}\right] R_O^{4(n+1)}}{\left[1-4\,(2n+1)^2\right]\left(R_O^2 - R_I^2\right)^2 - \left[R_O^{2(4n+3)} - R_I^{2(4n+3)}\right]\left[R_O^{-2(4n+1)} - R_I^{-2(4n+1)}\right]}$$

$$\cdot \left[\cos 2\,(2n+1)\,\phi_o - i \sin 2\,(2n+1)\,\phi_o\right],$$

$$B_{-2(2n+1)} = \left[\frac{\sin 2\,(2n+1)\,\omega_o}{2\,(2n+1)\sin^2\omega_o} + \frac{\sin 2\omega_o \cos 2\,(2n+1)\,\omega_o - (2n+1)\cos 2\omega_o \sin 2\,(2n+1)\,\omega_o}{8n\,(n+1)\sin^2\omega_o} - \frac{\sin 2\,(2n+1)\,\omega_o}{2n+1} \right]$$

$$\cdot \frac{(4n+1)\left(R_I^2 - R_O^2\right) R_O^{4(n+1)} + \left[R_I^{2(4n+3)} - R_O^{2(4n+3)}\right] R_O^{-4n}}{\left[1-4\,(2n+1)^2\right]\left(R_O^2 - R_I^2\right)^2 - \left[R_O^{2(4n+3)} - R_I^{2(4n+3)}\right]\left[R_O^{-2(4n+1)} - R_I^{-2(4n+1)}\right]}$$

$$\cdot \left[\cos 2\,(2n+1)\,\phi_o + i \sin 2\,(2n+1)\,\phi_o\right],$$

$$B_0' = \left(\frac{\omega_o - \sin 2\omega_o}{\sin^2\omega_o} + \frac{\sin 2\omega_o \cos 2\omega_o}{2\sin^2\omega_o} + 2\sin 2\omega_o \right) \cdot \frac{R_I^2\left(2R_I^2 - R_O^2 - R_O^6 R_I^{-4}\right)}{3\left(R_O^2 - R_I^2\right)^2 + \left(R_O^6 - R_I^6\right)\left(R_O^{-2} - R_I^{-2}\right)} \left(\cos 2\phi_o - i \sin 2\phi_o\right),$$

$$B_2' = \left(\frac{\sin 4\omega_o}{\sin^2\omega_o} + 2\frac{\sin 2\omega_o \cos 4\omega_o - 2\cos 2\omega_o \sin 4\omega_o}{3\sin^2\omega_o} - 2\sin 4\omega_o \right) \cdot \frac{R_I^2\left(3 - 4R_O^{-2}R_I^2 + R_O^8 R_I^{-8}\right)}{15\left(R_O^2 - R_I^2\right)^2 + \left(R_O^{10} - R_I^{10}\right)\left(R_O^{-6} - R_I^{-6}\right)} \left(\cos 4\phi_o - i \sin 4\phi_o\right),$$

$$b'_{-2}=\left(\frac{2\omega_o-\sin 2\omega_o}{2\sin^2\omega_o}-2\omega_o\right)\frac{R_O^2R_I^2}{R_O^2-R_I^2},$$

$$B'_{-4}=\left(\frac{\omega_o-\sin 2\omega_o}{\sin^2\omega_o}+\frac{\sin 2\omega_o\cos 2\omega_o}{2\sin^2\omega_o}+2\sin 2\omega_o\right)$$
$$\cdot\frac{R_O^2R_I^2\left(R_I^4+2R_O^2R_I^2-3R_O^4\right)}{3\left(R_O^2-R_I^2\right)^2+\left(R_O^6-R_I^6\right)\left(R_O^{-2}-R_I^{-2}\right)}\cdot(\cos 2\phi_o+i\sin 2\phi_o),$$

$$B'_{4n}=\left[\frac{\sin 2\left(2n+1\right)\omega_o}{2\left(2n+1\right)\sin^2\omega_o}\right.$$
$$\left.+\frac{\sin 2\omega_o\cos 2\left(2n+1\right)\omega_o-\left(2n+1\right)\cos 2\omega_o\sin 2\left(2n+1\right)\omega_o}{8n\left(n+1\right)\sin^2\omega_o}-\frac{\sin 2\left(2n+1\right)\omega_o}{2n+1}\right]$$
$$\cdot\left\{\left(4n+1\right)R_I^2\left[\left(4n+3\right)\left(R_I^2-R_O^2\right)R_O^{-4n}-\left[R_I^{-2(4n+1)}-R_O^{-2(4n+1)}\right]R_O^{4(n+1)}\right]\right.$$
$$\left.+\,R_I^{-2(4n+1)}\left[\left(4n+1\right)\left(R_I^2-R_O^2\right)R_O^{4(n+1)}+\left[R_I^{2(4n+3)}-R_O^{2(4n+3)}\right]R_O^{-4n}\right]\right\}$$
$$\Big/\left\{\left[1-4\left(2n+1\right)^2\right]\left(R_O^2-R_I^2\right)^2-\left[R_O^{2(4n+3)}-R_I^{2(4n+3)}\right]\right.$$
$$\left.\cdot\left[R_O^{-2(4n+1)}-R_I^{-2(4n+1)}\right]\right\}\cdot\left[\cos 2\left(2n+1\right)\phi_o-i\sin 2\left(2n+1\right)\phi_o\right],$$

$$B'_{2(2n+1)}=\left[\frac{\sin 4\left(n+1\right)\omega_o}{4\left(n+1\right)\sin^2\omega_o}\right.$$
$$\left.+\,\frac{\sin 2\omega_o\cos 4\left(n+1\right)\omega_o-2\left(n+1\right)\cos 2\omega_o\sin 4\left(n+1\right)\omega_o}{2\left[4\left(n+1\right)^2-1\right]\sin^2\omega_o}-\frac{\sin 4\left(n+1\right)\omega_o}{2\left(n+1\right)}\right]$$
$$\cdot\left\{\left(4n+3\right)R_I^2\left[\left(4n+5\right)\left(R_I^2-R_O^2\right)R_O^{-2(2n+1)}-\left[R_I^{-2(4n+3)}-R_O^{-2(4n+3)}\right]R_O^{2(2n+3)}\right]\right.$$
$$\left.+\,R_I^{-2(4n+3)}\left[\left(4n+3\right)\left(R_I^2-R_O^2\right)R_O^{2(2n+3)}+\left[R_I^{2(4n+5)}-R_O^{2(4n+5)}\right]R_O^{-2(2n+1)}\right]\right\}$$
$$\Big/\left\{\left[1-16\left(n+1\right)^2\right]\left(R_O^2-R_I^2\right)^2-\left[R_O^{2(4n+5)}-R_I^{2(4n+5)}\right]\right.$$
$$\left.\cdot\left[R_O^{-2(4n+3)}-R_I^{-2(4n+3)}\right]\right\}\cdot\left[\cos 4\left(n+1\right)\phi_o-i\sin 4\left(n+1\right)\phi_o\right],$$

$$B'_{-4(n+1)} = \left[\frac{\sin 2\,(2n+1)\,\omega_o}{2\,(2n+1)\sin^2\omega_o}\right.$$

$$\left.+\frac{\sin 2\omega_o \cos 2\,(2n+1)\,\omega_o - (2n+1)\cos 2\omega_o \sin 2\,(2n+1)\,\omega_o}{8n\,(n+1)\sin^2\omega_o} - \frac{\sin 2\,(2n+1)\,\omega_o}{2n+1}\right]$$

$$\cdot\left\{(4n+3)\,R_I^2\left[(4n+1)\left(R_I^2-R_O^2\right)R_O^{4(n+1)} + \left[R_I^{2(4n+3)} - R_O^{2(4n+3)}\right]R_O^{-4n}\right]\right.$$

$$\left.- R_I^{2(4n+3)}\left[(4n+3)\left(R_I^2-R_O^2\right)R_O^{-4n} - \left[R_I^{-2(4n+1)} - R_O^{-2(4n+1)}\right]R_O^{4(n+1)}\right]\right\}$$

$$\Big/\left\{\left[1-4\,(2n+1)^2\right]\left(R_O^2-R_I^2\right)^2 - \left[R_O^{2(4n+3)} - R_I^{2(4n+3)}\right]\right.$$

$$\left.\cdot\left[R_O^{-2(4n+1)} - R_I^{-2(4n+1)}\right]\right\}\cdot\left[\cos 2\,(2n+1)\,\phi_o + i\sin 2\,(2n+1)\,\phi_o\right],$$

$$B'_{-2(2n+1)} = \left[\frac{\sin 4n\omega_o}{4n\sin^2\omega_o} + \frac{\sin 2\omega_o\cos 4n\omega_o - 2n\cos 2\omega_o\sin 4n\omega_o}{2\,(4n^2-1)\sin^2\omega_o} - \frac{\sin 4n\omega_o}{2n}\right]$$

$$\cdot\left\{(1+4n)\,R_I^2\left[(1-4n)\left(R_O^2-R_I^2\right)R_O^{2(2n+1)} - \left[R_O^{2(4n+1)} - R_I^{2(4n+1)}\right]R_O^{-2(2n-1)}\right]\right.$$

$$+ R_I^{2(4n+1)}\left[(1+4n)\left(R_O^2-R_I^2\right)R_O^{-2(2n-1)} - \left[R_O^{-2(4n-1)} - R_I^{-2(4n-1)}\right]R_O^{2(2n+1)}\right]\Big\}$$

$$\Big/\left\{\left(1-16n^2\right)\left(R_O^2-R_I^2\right)^2 - \left[R_O^{2(4n+1)} - R_I^{2(4n+1)}\right]\left[R_O^{-2(4n-1)} - R_I^{-2(4n-1)}\right]\right\}$$

$$\cdot\left(\cos 4n\phi_o + i\sin 4n\phi_o\right),$$

Appendix B. a) The principal parts, i.e. parts of the following functions in brackets that spawn poles at the point at infinity and at $\zeta = 0$, entering in Eqs. (3.7), (3.8)

$$G^{\infty}_{4n+1}(\zeta) := \underset{\zeta=\infty}{P.P.}\left(\zeta + \frac{m}{\zeta}\right)^{4n+1} = \sum_{k=0}^{2n}\frac{(4n+1)!}{k!\,(4n+1-k)!}m^k\zeta^{2(2n-k)+1},$$

$$G^{\infty}_{4n+3}(\zeta) := \underset{\zeta=\infty}{P.P.}\left(\zeta + \frac{m}{\zeta}\right)^{4n+3} = \sum_{k=0}^{2n+1}\frac{(4n+3)!}{k!\,(4n+3-k)!}m^k\zeta^{2(2n-k)+3},$$

$$G_{4n}^{0}\left(\zeta\right):=\underset{\zeta=0}{P.P.}\left(\frac{1}{\zeta}+m\zeta\right)^{4n}=\sum_{k=0}^{2n-1}\frac{(4n)!}{k!\,(4n-k)!}m^{k}\zeta^{2(k-2n)+1}$$

$$+\sum_{k=0}^{2n}\frac{(4n)!}{k!\,(4n-k)!}m^{k+1}\zeta^{2(k-2n)-1},$$

$$G_{2(2n+1)}^{0}\left(\zeta\right):=\underset{\zeta=0}{P.P.}\left(\frac{1}{\zeta}+m\zeta\right)^{2(2n+1)}=\sum_{k=0}^{2n}\frac{[2\,(2n+1)]!}{k!\,[2\,(2n+1)-k]!}m^{k}\zeta^{2(k-2n)-1}$$

$$+\sum_{k=0}^{2n+1}\frac{[2\,(2n+1)]!}{k!\,[2\,(2n+1)-k]!}m^{k+1}\zeta^{2(k-2n)-3},$$

$$G_{4n+1}^{0}\left(\zeta\right):=\underset{\zeta=0}{P.P.}\left(\frac{1}{\zeta}+m\zeta\right)^{4n+1}=\sum_{k=0}^{2n}\frac{(4n+1)!}{k!\,(4n+1-k)!}m^{k}\zeta^{2(k-2n)-1},$$

$$G_{4n+3}^{0}\left(\zeta\right):=\underset{\zeta=\,0}{P.P.}\left(\frac{1}{\zeta}+m\zeta\right)^{4n+3}=\sum_{k=0}^{2n+1}\frac{(4n+3)!}{k!\,(4n+3-k)!}m^{k}\zeta^{2(k-2n)-3},$$

$$G_{4n}^{\infty}\left(\zeta\right):=\underset{\zeta=\infty}{P.P.}\left(\zeta+\frac{m}{\zeta}\right)^{4n}=\sum_{k=0}^{2n-1}\frac{(4n)!}{k!\,(4n-k)!}m^{k}\zeta^{2(2n-k)-1}$$

$$+\sum_{k=0}^{2n}\frac{(4n)!}{k!\,(4n-k)!}m^{k+1}\zeta^{2(2n-k)+1},$$

$$G_{2(2n+1)}^{\infty}\left(\zeta\right):=\underset{\zeta=\infty}{P.P.}\left(\zeta+\frac{m}{\zeta}\right)^{2(2n+1)}=\sum_{k=0}^{2n}\frac{[2\,(2n+1)]!}{k!\,[2\,(2n+1)-k]!}m^{k}\zeta^{2(2n-k)+1}$$

$$+\sum_{k=0}^{2n+1}\frac{[2\,(2n+1)]!}{k!\,[2\,(2n+1)-k]!}\,m^{k+1}\,\zeta^{2(2n-k)+3},$$

B) DEALING WITH CAUCHY TYPE INTEGRALS WHILE OBTAINING $\varphi_*(\zeta)$, $\psi_*(\zeta)$

To obtain $\dfrac{1}{2\pi i}\displaystyle\int_\gamma \frac{f_*(s)ds}{s-\zeta}$ (first of Eqs. (3.6)) one has to deal with the integral

$$\frac{1}{2\pi i}\int_\gamma \sum_{n=1}^{\infty} \frac{B_{4n}}{4n+1} R^{4n+1}\left(s+\frac{m}{s}\right)^{4n+1} \frac{ds}{s-\zeta}.$$

The quantity $\left(s+\dfrac{m}{s}\right)^{4n+1}$ appearing in this integral is the boundary value of the function $\left(\zeta+\dfrac{m}{\zeta}\right)^{4n+1}$ on γ. This function is holomorphic outside γ and has a pole at infinity denoted by $G^{\infty}_{4n+1}(\zeta)$. Then, based on properties of Cauchy type integrals, we find

$$\frac{1}{2\pi i}\int_\gamma \sum_{n=1}^{\infty} \frac{B_{4n}}{4n+1} R^{4n+1}\left(s+\frac{m}{s}\right)^{4n+1} \frac{ds}{s-\zeta}$$
$$= \sum_{n=1}^{\infty} \frac{B_{4n}}{4n+1} R^{4n+1}\left[-\left(\zeta+\frac{m}{\zeta}\right)^{4n+1} + G^{\infty}_{4n+1}(\zeta)\right].$$

C) THE DERIVATION OF THE EXPRESSION FOR $G^{\infty}_{4n+1}(\zeta)$

To derive the analytic expression for

$$G^{\infty}_{4n+1}(\zeta) := \underset{\zeta=\infty}{P.P.}\left(\zeta+\frac{m}{\zeta}\right)^{4n+1}$$

(the first formula of Appendix B(a)) use is made of the formula $(a+b)^{\ell} = \displaystyle\sum_{k=0}^{\ell} \frac{\ell!}{k!\,(\ell-k)!} a^{\ell-k}b^k$ (obtained by the factorial function $\dfrac{\ell!}{k!(\ell-k)!}$ or by Pascal's Triangle). Thus, substituting $a=\zeta$, $b=m/\zeta$ and $\ell = 4n+1$, and by keeping only that part of the expansion which provides poles at infinity, one obtains

$$G^{\infty}_{4n+1}(\zeta) := \underset{\zeta=\infty}{P.P.}\left(\zeta+\frac{m}{\zeta}\right)^{4n+1} = \sum_{k=0}^{2n} \frac{(4n+1)!}{k!\,(4n+1-k)!} m^k \zeta^{2(2n-k)+1}$$

that is the first formula of Appendix B(a) which had to be derived.

Appendix C. The Cartesian components of the stress field along x-axis aligned to the major axis α of the elliptical hole

$$
\begin{aligned}
\text{(C.1)}\quad \left.\begin{matrix}\sigma_x\\ \sigma_y\end{matrix}\right\} &= \frac{2P_c}{\pi}\frac{\xi^2}{\xi^2-m}\Bigg\{\Re\left(mB_2+\frac{B_2'}{3}\right)\frac{3R^2}{\xi^4} \\
&\quad +\frac{mb_0+\Re B_0'+R^2\Re\left[(1+2m^2)B_2+mB_2'\right]}{\xi^2}+R^2\Re B_2(m+\xi^2)+b_0 \\
&\quad +\sum_{n=1}^{\infty}R^{4n}\Bigg[\Re B_{4n}\left(\frac{1}{4n+1}\frac{dG_{4n+1}^{\infty}}{d\zeta}(\xi)-\frac{dG_{4n}^{0}}{d\zeta}(\xi)\right)-\frac{\Re B_{4n}'}{4n+1}\frac{dG_{4n+1}^{0}}{d\zeta}(\xi) \\
&\quad +R^2\left(\Re B_{2(2n+1)}\left(\frac{1}{4n+3}\frac{dG_{4n+3}^{\infty}}{d\zeta}(\xi)-\frac{dG_{2(2n+1)}^{0}}{d\zeta}(\xi)\right)-\frac{\Re B_{2(2n+1)}'}{4n+3}\frac{dG_{4n+3}^{0}}{d\zeta}(\xi)\right)\Bigg]\Bigg\} \\
&\quad \mp\frac{P_c}{\pi}\frac{\xi^2}{(\xi^2-m)^3}\Bigg\{3\Re B_0'+R^2\Re B_2\left[m\left(\frac{6m^2-8m}{\xi^4}-\frac{6m-13.33}{\xi^2}-12\right)+4(1+3m^2)\right] \\
&\quad +R^2\Re B_2'\left(\frac{2m^2-3m}{\xi^4}-\frac{2m-5}{\xi^2}+6m-4\right)-\frac{m}{\xi^2}\Re\left[\frac{4(1+3m^2)R^2B_2}{3}+B_0'+2mR^2B_2'\right] \\
&\quad +R^2\Re B_2'\left(\xi^6-\frac{5m\xi^4}{3}\right)+\Re\left(B_0'+\frac{2mR^2B_2'}{3}\right)(\xi^4-3m\xi^2)+2R^2\Re B_2(\xi^6-m\xi^4-3m^2\xi^2-m^3) \\
&\quad +2(\xi^2+m)\left[(1-m)^2b_0+R^2(2m+2m^3-2m^2-1)\Re B_2+(m-1)\left(\Re B_0'+mR^2\Re B_2'\right)\right] \\
&\quad +\left[m\left(1-2m\right)-m\xi^4+\left(1-2m+3m^2\right)\xi^2\right] \\
&\quad \cdot\sum_{n=1}^{\infty}R^{4n}\Bigg[\Re B_{4n}\left(\frac{1}{4n+1}\frac{dG_{4n+1}^{\infty}}{d\zeta}(\xi)-\frac{dG_{4n}^{0}}{d\zeta}(\xi)\right)-\frac{\Re B_{4n}'}{4n+1}\frac{dG_{4n+1}^{0}}{d\zeta}(\xi) \\
&\quad +R^2\left(\Re B_{2(2n+1)}\left(\frac{1}{4n+3}\frac{dG_{4n+3}^{\infty}}{d\zeta}(\xi)-\frac{dG_{2(2n+1)}^{0}}{d\zeta}(\xi)\right)-\frac{\Re B_{2(2n+1)}'}{4n+3}\frac{dG_{4n+3}^{0}}{d\zeta}(\xi)\right)\Bigg] \\
&\quad +\left[m(1-m)\xi-(1-m^2)\xi^3+(1-m)\xi^5\right] \\
&\quad \cdot\sum_{n=1}^{\infty}R^{4n}\Bigg[\Re B_{4n}\left(\frac{1}{4n+1}\frac{d^2G_{4n+1}^{\infty}}{d\zeta^2}(\xi)-\frac{d^2G_{4n}^{0}}{d\zeta^2}(\xi)\right)-\frac{\Re B_{4n}'}{4n+1}\frac{d^2G_{4n+1}^{0}}{d\zeta^2}(\xi) \\
&\quad +R^2\left(\Re B_{2(2n+1)}\left(\frac{1}{4n+3}\frac{d^2G_{4n+3}^{\infty}}{d\zeta^2}(\xi)-\frac{d^2G_{2(2n+1)}^{0}}{d\zeta^2}(\xi)\right)-\frac{\Re B_{2(2n+1)}'}{4n+3}\frac{d^2G_{4n+3}^{0}}{d\zeta^2}(\xi)\right)\Bigg] \\
&\quad +(m-\xi^2)^2\sum_{n=1}^{\infty}R^{4n}\Bigg[\Re B_{4n}\left(\frac{dG_{4n}^{\infty}}{d\zeta}(\xi)-\frac{1}{4n+1}\frac{dG_{4n+1}^{0}}{d\zeta}(\xi)\right)+\frac{\Re B_{4n}'}{4n+1}\frac{dG_{4n+1}^{\infty}}{d\zeta}(\xi) \\
&\quad +R^2\left(\Re B_{2(2n+1)}\left(\frac{dG_{2(2n+1)}^{\infty}}{d\zeta}(\xi)-\frac{1}{4n+3}\frac{dG_{4n+3}^{0}}{d\zeta}(\xi)\right)+\frac{\Re B_{2(2n+1)}'}{4n+3}\frac{dG_{4n+3}^{\infty}}{d\zeta}(\xi)\right)\Bigg]\Bigg\},
\end{aligned}
$$

$$
\begin{aligned}
(\mathrm{C.2})\quad \sigma_{xy} = \frac{P_c}{\pi}\frac{\xi^2}{(\xi^2-m)^3}\Bigg\{ & -3\Im B_0' \\
& - R^2\Im B_2\left[m\left(\frac{6m^2-8m}{\xi^4}-\frac{6m-13.33}{\xi^2}-12\right)+4(1+3m^2)\right] \\
& - R^2\Im B_2'\left(\frac{2m^2-3m}{\xi^4}-\frac{2m-5}{\xi^2}+6m-4\right) \\
& + \frac{m}{\xi^2}\Im\left[\frac{4(1+3m^2)R^2B_2}{3}+B_0'+2mR^2B_2'\right] \\
& + R^2\Im B_2'\left(\xi^6-\frac{5m\xi^4}{3}\right)+\Im\left(B_0'+\frac{2mR^2B_2'}{3}\right)(\xi^4-3m\xi^2) \\
& + 2R^2\Im B_2\left(\xi^6-m\xi^4-3m^2\xi^2-m^3\right) \\
& + 2(\xi^2+m)\Im\left[R^2(1+2m^2)B_2+B_0'+mR^2B_2'\right] \\
& + \left[m(1-2m)-m\xi^4+(1-2m+3m^2)\xi^2\right] \\
& \cdot\sum_{n=1}^{\infty}R^{4n}\left[\Im B_{4n}\left(\frac{1}{4n+1}\frac{dG_{4n+1}^{\infty}}{d\zeta}(\xi)+\frac{dG_{4n}^{0}}{d\zeta}(\xi)\right)+\frac{\Im B_{4n}'}{4n+1}\frac{dG_{4n+1}^{0}}{d\zeta}(\xi)\right. \\
& \left.+R^2\left(\Im B_{2(2n+1)}\left(\frac{dG_{2(2n+1)}^{0}}{d\zeta}(\xi)+\frac{1}{4n+3}\frac{dG_{4n+3}^{\infty}}{d\zeta}(\xi)\right)+\frac{\Im B_{2(2n+1)}'}{4n+3}\frac{dG_{4n+3}^{0}}{d\zeta}(\xi)\right)\right] \\
& + \left[m(1-m)\xi-(1-m^2)\xi^3+(1-m)\xi^5\right] \\
& \cdot\sum_{n=1}^{\infty}R^{4n}\left[\Im B_{4n}\left(\frac{1}{4n+1}\frac{d^2G_{4n+1}^{\infty}}{d\zeta^2}(\xi)+\frac{d^2G_{4n}^{0}}{d\zeta^2}(\xi)\right)+\frac{\Im B_{4n}'}{4n+1}\frac{d^2G_{4n+1}^{0}}{d\zeta^2}(\xi)\right. \\
& \left.+R^2\left(\Im B_{2(2n+1)}\left(\frac{d^2G_{2(2n+1)}^{0}}{d\zeta^2}(\xi)+\frac{1}{4n+3}\frac{d^2G_{4n+3}^{\infty}}{d\zeta^2}(\xi)\right)+\frac{\Im B_{2(2n+1)}'}{4n+3}\frac{d^2G_{4n+3}^{0}}{d\zeta^2}(\xi)\right)\right] \\
& + (m-\xi^2)^2\sum_{n=1}^{\infty}R^{4n}\left[\Im B_{4n}\left(\frac{dG_{4n}^{\infty}}{d\zeta}(\xi)+\frac{1}{4n+1}\frac{dG_{4n+1}^{0}}{d\zeta}(\xi)\right)\right. \\
& + \frac{\Im B_{4n}'}{4n+1}\frac{dG_{4n+1}^{\infty}}{d\zeta}(\xi)+R^2\left(\Im B_{2(2n+1)}\left(\frac{dG_{2(2n+1)}^{\infty}}{d\zeta}(\xi)+\frac{1}{4n+3}\frac{dG_{4n+3}^{0}}{d\zeta}(\xi)\right)\right. \\
& \left.\left.\left.+\frac{\Im B_{2(2n+1)}'}{4n+3}\frac{dG_{4n+3}^{\infty}}{d\zeta}(\xi)\right)\right]\Bigg\}.
\end{aligned}
$$

Appendix D. The explicit formulae of the displacement field

$$
\begin{aligned}
(\mathrm{D.1})\quad u_{\mathrm{eq}}(\rho,\theta) = \frac{P_c R}{2\pi\mu}\Bigg\{\kappa\Bigg[&\Re\left[(b_0+mR^2B_2)\rho\right.\\
&\left.-\left[mb_0+B_0'+R^2\left[(1+2m^2)B_2+mB_2'\right]\right]/\rho\right]\cos\theta\\
&+R^2\Re\left[\left(\rho^3/3-m/\rho^3\right)B_2-B_2'/(3\rho^3)\right]\cos 3\theta\\
&+\sum_{n=1}^{\infty}R^{4n}\left[\Re B_{4n}\left(\frac{\Re G^{\infty}_{4n+1}}{4n+1}-\Re G^{0}_{4n}\right)-\frac{\Re B'_{4n}\Re G^{0}_{4n+1}}{4n+1}\right.\\
&\left.+R^2\left(\Re B_{2(2n+1)}\left(\frac{\Re G^{\infty}_{4n+3}}{4n+3}-\Re G^{0}_{2(2n+1)}\right)-\frac{\Re B'_{2(2n+1)}\Re G^{0}_{4n+3}}{4n+3}\right)\right]\Bigg]-\frac{\rho\left(\rho^4\cos\theta-m^2\cos 3\theta\right)}{\rho^4+m^2-2m\rho^2\cos 2\theta}\\
&\cdot\Re\left[b_0+mR^2B_2+\left[R^2B_2\rho^2+\left[mb_0+B_0'+R^2\left[(1+2m^2)B_2+mB_2'\right]\right]/\rho^2\right]\cos 2\theta\right.\\
&\left.+R^2(3mB_2+B_2')\cos 4\theta/\rho^4\right]-\frac{\rho^2(\rho^2-m\cos 2\theta)}{\rho^4+m^2-2m\rho^2\cos 2\theta}\Re\left[\left[\left(B_0'+2mR^2B_2'/3\right)\rho\right.\right.\\
&\left.\left.-2\left[(1+m^2)(b_0+2mR^2B_2)+m(B_0'+mR^2B_2')\right]/\rho\right]\cos\theta-R^2\left(8mB_2/3+B_2'\right)\cos 5\theta/\rho^5\right.\\
&\left.+\left[R^2B_2'\rho^3/3-\left[R^2\left[4B_2(1+3m^2)/3+2mB_2'\right]+B_0'\right]/\rho^3\right]\cos 3\theta\right]+\rho\left[\left[\rho^4(1-m)-\rho^2+m\right]\cos\theta\right.\\
&\left.-m^2(1-\rho^2)\cos 3\theta\right]/(\rho^4+m^2-2m\rho^2\cos 2\theta)\cdot\sum_{n=1}^{\infty}R^{4n}\left[\Re B_{4n}\left(\Re\frac{dG^{0}_{4n}}{d\zeta}-\frac{1}{4n+1}\Re\frac{dG^{\infty}_{4n+1}}{d\zeta}\right)\right.\\
&\left.+\frac{\Re B'_{4n}}{4n+1}\Re\frac{dG^{0}_{4n+1}}{d\zeta}+R^2\left(\Re B_{2(2n+1)}\left(\Re\frac{dG^{0}_{2(2n+1)}}{d\zeta}-\frac{1}{4n+3}\Re\frac{dG^{\infty}_{4n+3}}{d\zeta}\right)+\frac{\Re B'_{2(2n+1)}}{4n+3}\Re\frac{dG^{0}_{4n+3}}{d\zeta}\right)\right]\\
&+\sum_{n=1}^{\infty}R^{4n}\left[\Re B_{4n}\left(\frac{\Re G^{0}_{4n+1}}{4n+1}-\Re G^{\infty}_{4n}\right)-\frac{\Re B'_{4n}\Re G^{\infty}_{4n+1}}{4n+1}\right.\\
&\left.+R^2\left(\Re B_{2(2n+1)}\left(\frac{\Re G^{0}_{4n+3}}{4n+3}-\Re G^{\infty}_{2(2n+1)}\right)-\frac{\Re B'_{2(2n+1)}\Re G^{\infty}_{4n+3}}{4n+3}\right)\right]\\
&+\frac{\rho(\rho^4\sin\theta+m^2\sin 3\theta)}{\rho^4+m^2-2m\rho^2\cos 2\theta}\Re\left[\left[mb_0+B_0'+R^2\left[(1+2m^2)B_2+mB_2'\right]\right]\sin 2\theta/\rho^2-R^2B_2\rho^2\right.\\
&\left.+R^2(3mB_2+B_2')\sin 4\theta/\rho^4\right]-\frac{m\rho^2\sin 2\theta}{\rho^4+m^2-2m\rho^2\cos 2\theta}\Re\left[\left[\left(B_0'+2mR^2B_2'/3\right)\rho\right.\right.\\
&\left.\left.+2\left[(1+m^2)(b_0+2mR^2B_2)+m(B_0'+mR^2B_2')\right]/\rho\right]\sin\theta+R^2\left(8mB_2/3+B_2'\right)\sin 5\theta/\rho^5\right.\\
&\left.+\left[R^2B_2'\rho^3/3+\left[R^2\left[4B_2(1+3m^2)/3+2mB_2'\right]+B_0'\right]/\rho^3\right]\sin 3\theta\right]\\
&+\rho\left[\left[\rho^4(1+m)-\rho^2-m\right]\sin\theta+m^2(1-\rho^2)\sin 3\theta\right]/\left(\rho^4+m^2-2m\rho^2\cos 2\theta\right)\\
&\cdot\sum_{n=1}^{\infty}R^{4n}\left[\Re B_{4n}\left(\Im\frac{dG^{0}_{4n}}{d\zeta}-\frac{1}{4n+1}\Im\frac{dG^{\infty}_{4n+1}}{d\zeta}\right)+\frac{\Re B'_{4n}}{4n+1}\Im\frac{dG^{0}_{4n+1}}{d\zeta}\right.\\
&\left.+R^2\left(\Re B_{2(2n+1)}\left(\Im\frac{dG^{0}_{2(2n+1)}}{d\zeta}-\frac{1}{4n+3}\Im\frac{dG^{\infty}_{4n+3}}{d\zeta}\right)+\frac{\Re B'_{2(2n+1)}}{4n+3}\Im\frac{dG^{0}_{4n+3}}{d\zeta}\right)\right]\Bigg\},
\end{aligned}
$$

$$
\begin{aligned}
(\mathrm{D.2}) \quad u_{\mathrm{op}}(\rho,\theta) = \frac{P_c R}{2\pi\mu}\Bigg\{ \kappa \Bigg[& \Im\left[\left[B_0' + R^2\left[\left(1+2m^2\right)B_2 + mB_2'\right]\right]/\rho - mR^2 B_2 \rho\right]\sin\theta \\
& - R^2 \Im\left[\left(\rho^3/3 - m/\rho^3\right)B_2 - B_2'/\left(3\rho^3\right)\right]\sin 3\theta - \sum_{n=1}^{\infty} R^{4n}\left[\Im B_{4n}\left(\frac{\Im G_{4n+1}^{\infty}}{4n+1} + \Im G_{4n}^{0}\right)\right. \\
& \left. + \frac{\Im B_{4n}' \Im G_{4n+1}^{0}}{4n+1} + R^2\left(\Im B_{2(2n+1)}\left(\frac{\Im G_{4n+3}^{\infty}}{4n+3} + \Im G_{2(2n+1)}^{0}\right) + \frac{\Im B_{2(2n+1)}' \Im G_{4n+3}^{0}}{4n+3}\right)\right]\Bigg] \\
& - \frac{\rho\left(\rho^4 \sin\theta + m^2 \sin 3\theta\right)}{\rho^4 + m^2 - 2m\rho^2\cos 2\theta}\Im\left[mR^2 B_2 + \left[R^2 B_2 \rho^2 - \left[B_0' + R^2\left[\left(1+2m^2\right)B_2 + mB_2'\right]\right]/\rho^2\right]\cos 2\theta\right. \\
& \left. - R^2\left(3mB_2 + B_2'\right)\cos 4\theta/\rho^4\right] + \frac{\rho^2\left(\rho^2 - m\cos 2\theta\right)}{\rho^4 + m^2 - 2m\rho^2\cos 2\theta}\Im\left[\left(B_0' + 2mR^2 B_2'/3\right)\rho\sin\theta\right. \\
& \left. - R^2\left(8mB_2/3 + B_2'\right)\sin 5\theta/\rho^5 + \left[R^2 B_2' \rho^3/3 - \left[R^2\left[4B_2\left(1+3m^2\right)/3 + 2mB_2'\right] + B_0'\right]/\rho^3\right]\sin 3\theta\right] \\
& + \rho\left[\left[\rho^4(1-m) - \rho^2 + m\right]\cos\theta - m^2\left(1-\rho^2\right)\cos 3\theta\right]/\left(\rho^4 + m^2 - 2m\rho^2\cos 2\theta\right) \\
& \cdot \sum_{n=1}^{\infty} R^{4n}\left[\Im B_{4n}\left(\Im\frac{dG_{4n}^{0}}{d\zeta} + \frac{1}{4n+1}\Im\frac{dG_{4n+1}^{\infty}}{d\zeta}\right) + \frac{\Im B_{4n}'}{4n+1}\Im\frac{dG_{4n+1}^{0}}{d\zeta}\right. \\
& \left. + R^2\left(\Im B_{2(2n+1)}\left(\Im\frac{dG_{2(2n+1)}^{0}}{d\zeta} + \frac{1}{4n+3}\Im\frac{dG_{4n+3}^{\infty}}{d\zeta}\right) + \frac{\Im B_{2(2n+1)}'}{4n+3}\Im\frac{dG_{4n+3}^{0}}{d\zeta}\right)\right] \\
& + \sum_{n=1}^{\infty} R^{4n}\left[\Im B_{4n}\left(\frac{\Im G_{4n+1}^{0}}{4n+1} + \Im G_{4n}^{\infty}\right) + \frac{\Im B_{4n}' \Im G_{4n+1}^{\infty}}{4n+1}\right. \\
& \left. + R^2\left(\Im B_{2(2n+1)}\left(\frac{\Im G_{4n+3}^{0}}{4n+3} + \Im G_{2(2n+1)}^{\infty}\right)\right.\right. \\
& \left.\left. + \frac{\Im B_{2(2n+1)}' \Im G_{4n+3}^{\infty}}{4n+3}\right)\right] + \frac{\rho\left(\rho^4\cos\theta - m^2\cos 3\theta\right)}{\rho^4 + m^2 - 2m\rho^2\cos 2\theta}\Im\left[\left[R^2 B_2\rho^2\right.\right. \\
& \left.\left. + \left[B_0' + R^2\left[\left(1+2m^2\right)B_2 + mB_2'\right]\right]/\rho^2\right]\sin 2\theta + R^2\left(3mB_2 + B_2'\right)\sin 4\theta/\rho^4\right] \\
& - \frac{m\rho^2\sin 2\theta}{\rho^4 + m^2 - 2m\rho^2\cos 2\theta}\Im\left[\left[\left(B_0' + 2mR^2 B_2'/3\right)\rho\cos\theta + \left[R^2 B_2'\rho^3/3\right.\right.\right. \\
& \left.\left.\left. + \left[R^2\left[4B_2\left(1+3m^2\right)/3 + 2mB_2'\right] + B_0'\right]/\rho^3\right]\cos 3\theta\right] + R^2\left(8mB_2/3 + B_2'\right)\cos 5\theta/\rho^5\right] \\
& - \rho\left[\left[\rho^4(1+m) - \rho^2 - m\right]\sin\theta + m^2\left(1-\rho^2\right)\sin 3\theta\right]/\left(\rho^4 + m^2 - 2m\rho^2\cos 2\theta\right) \\
& \cdot \sum_{n=1}^{\infty} R^{4n}\left[\Im B_{4n}\left(\Re\frac{dG_{4n}^{0}}{d\zeta} + \frac{1}{4n+1}\Re\frac{dG_{4n+1}^{\infty}}{d\zeta}\right) + \frac{\Im B_{4n}'}{4n+1}\Re\frac{dG_{4n+1}^{0}}{d\zeta}\right. \\
& \left. + R^2\left(\Im B_{2(2n+1)}\left(\Re\frac{dG_{2(2n+1)}^{0}}{d\zeta} + \frac{1}{4n+3}\Re\frac{dG_{4n+3}^{\infty}}{d\zeta}\right) + \frac{\Im B_{2(2n+1)}'}{4n+3}\Re\frac{dG_{4n+3}^{0}}{d\zeta}\right)\right]\Bigg\},
\end{aligned}
$$

$$
\begin{aligned}
(\mathrm{D.3}) \quad v_{\mathrm{eq}}(\rho,\theta) = \frac{P_c R}{2\pi\mu}\Bigg\{ \kappa \Bigg[& \Im\left[mR^2B_2\rho - \left[B_0' + R^2\left[\left(1+2m^2\right)B_2 + mB_2'\right]\right]/\rho\right]\cos\theta \\
& + R^2\Im\left[\left(\rho^3/3 + m/\rho^3\right)B_2 + B_2'/\left(3\rho^3\right)\right]\cos 3\theta + \sum_{n=1}^{\infty} R^{4n}\left[\Im B_{4n}\left(\frac{\Re G_{4n+1}^{\infty}}{4n+1} + \Re G_{4n}^{0}\right)\right. \\
& \left. + \frac{\Im B_{4n}'\Re G_{4n+1}^{0}}{4n+1} + R^2\left(\Im B_{2(2n+1)}\left(\frac{\Re G_{4n+3}^{\infty}}{4n+3} + \Re G_{2(2n+1)}^{0}\right) + \frac{\Im B_{2(2n+1)}'\Re G_{4n+3}^{0}}{4n+3}\right)\right]\Bigg] \\
& + \frac{\rho\left(\rho^4\cos\theta - m^2\cos 3\theta\right)}{\rho^4+m^2-2m\rho^2\cos 2\theta}\Im\left[mR^2B_2 + \left[R^2B_2\rho^2 - \left[B_0' + R^2\left[\left(1+2m^2\right)B_2 + mB_2'\right]\right]/\rho^2\right]\cos 2\theta\right. \\
& \left. - R^2\left(3mB_2 + B_2'\right)\cos 4\theta/\rho^4\right] + \frac{\rho^2\left(\rho^2 - m\cos 2\theta\right)}{\rho^4 + m^2 - 2m\rho^2\cos 2\theta}\Im\left[\left[\left(B_0' + 2mR^2B_2'/3\right)\rho\cos\theta\right.\right. \\
& \left.\left. + R^2(8mB_2/3 + B_2')\cos 5\theta/\rho^5 + \left[R^2B_2'\rho^3/3 + \left[R^2\left[4B_2\left(1+3m^2\right)/3 + 2mB_2'\right] + B_0'\right]/\rho^3\right]\cos 3\theta\right] \\
& + \rho\left[\left[\rho^4(1-m) - \rho^2 + m\right]\cos\theta - m^2\left(1-\rho^2\right)\cos 3\theta\right]/\left(\rho^4 + m^2 - 2m\rho^2\cos 2\theta\right) \\
& \cdot \sum_{n=1}^{\infty} R^{4n}\left[\Im B_{4n}\left(\Re\frac{dG_{4n}^{0}}{d\zeta} + \frac{1}{4n+1}\Re\frac{dG_{4n+1}^{\infty}}{d\zeta}\right) + \frac{\Im B_{4n}'}{4n+1}\Re\frac{dG_{4n+1}^{0}}{d\zeta}\right. \\
& \left. + R^2\left(\Im B_{2(2n+1)}\left(\Re\frac{dG_{2(2n+1)}^{0}}{d\zeta} + \frac{1}{4n+3}\Re\frac{dG_{4n+3}^{\infty}}{d\zeta}\right) + \frac{\Im B_{2(2n+1)}'}{4n+3}\Re\frac{dG_{4n+3}^{0}}{d\zeta}\right)\right] \\
& + \sum_{n=1}^{\infty} R^{4n}\left[\Im B_{4n}\left(\frac{\Re G_{4n+1}^{0}}{4n+1} + \Re G_{4n}^{\infty}\right) + \frac{\Im B_{4n}'\Re G_{4n+1}^{\infty}}{4n+1}\right. \\
& \left. + R^2\left(\Im B_{2(2n+1)}\left(\frac{\Re G_{4n+3}^{0}}{4n+3} + \Re G_{2(2n+1)}^{\infty}\right) + \frac{\Im B_{2(2n+1)}'\Re G_{4n+3}^{\infty}}{4n+3}\right)\right] \\
& + \frac{\rho\left(\rho^4\sin\theta + m^2\sin 3\theta\right)}{\rho^4 + m^2 - 2m\rho^2\cos 2\theta}\Im\left[\left[B_0' + R^2\left[\left(1+2m^2\right)B_2 + mB_2'\right]\right]\sin 2\theta/\rho^2 + R^2B_2\rho^2\right. \\
& \left. + R^2\left(3mB_2 + B_2'\right)\sin 4\theta/\rho^4\right] + \frac{m\rho^2\sin 2\theta}{\rho^4 + m^2 - 2m\rho^2\cos 2\theta}\Im\left[\left[\left(B_0' + 2mR^2B_2'/3\right)\rho\sin\theta\right.\right. \\
& \left.\left. - R^2(8mB_2/3 + B_2')\sin 5\theta/\rho^5 + \left[R^2B_2'\rho^3/3 - \left[R^2\left[4B_2\left(1+3m^2\right)/3 + 2mB_2'\right] + B_0'\right]/\rho^3\right]\sin 3\theta\right] \\
& + \rho\left[\left[\rho^4(1+m) - \rho^2 - m\right]\sin\theta + m^2\left(1-\rho^2\right)\sin 3\theta\right]/\left(\rho^4 + m^2 - 2m\rho^2\cos 2\theta\right) \\
& \cdot \sum_{n=1}^{\infty} R^{4n}\left[\Im B_{4n}\left(\Im\frac{dG_{4n}^{0}}{d\zeta} + \frac{1}{4n+1}\Im\frac{dG_{4n+1}^{\infty}}{d\zeta}\right) + \frac{\Im B_{4n}'}{4n+1}\Im\frac{dG_{4n+1}^{0}}{d\zeta}\right. \\
& \left.\left. + R^2\left(\Im B_{2(2n+1)}\left(\Im\frac{dG_{2(2n+1)}^{0}}{d\zeta} + \frac{1}{4n+3}\Im\frac{dG_{4n+3}^{\infty}}{d\zeta}\right) + \frac{\Im B_{2(2n+1)}'}{4n+3}\Im\frac{dG_{4n+3}^{0}}{d\zeta}\right)\right]\right\},
\end{aligned}
$$

$$
\begin{aligned}
(\mathrm{D.4}) \quad v_{\mathrm{op}}(\rho,\theta) = \frac{P_c R}{2\pi\mu}\Bigg\{ \kappa \Bigg[& \Re\left[\left[mb_o + B_0' + R^2\left[\left(1+2m^2\right)B_2 + mB_2'\right]\right]/\rho\right. \\
& \left. + \left(b_o + mR^2 B_2\right)\rho\right]\sin\theta + R^2\Re\left[\left(\rho^3/3 + m/\rho^3\right)B_2 + B_2'/\left(3\rho^3\right)\right]\sin 3\theta \\
& + \sum_{n=1}^{\infty} R^{4n}\left[\Re B_{4n}\left(\frac{\Im G_{4n+1}^{\infty}}{4n+1} - \Im G_{4n}^{0}\right) - \frac{\Re B_{4n}'\Im G_{4n+1}^{0}}{4n+1}\right. \\
& \left. + R^2\left(\Re B_{2(2n+1)}\left(\frac{\Im G_{4n+3}^{\infty}}{4n+3} - \Im G_{2(2n+1)}^{0}\right) - \frac{\Re B_{2(2n+1)}'\Im G_{4n+3}^{0}}{4n+3}\right)\right]\Bigg] \\
& + \frac{\rho\left(\rho^4\cos\theta - m^2\cos 3\theta\right)}{\rho^4 + m^2 - 2m\rho^2\cos 2\theta}\Re\left[R^2 B_2\rho^2 - \left[mb_o + B_0' + R^2\left[\left(1+2m^2\right)B_2 + mB_2'\right]\right]/\rho^2\right]\sin 2\theta \\
& - R^2\left(3mB_2 + B_2'\right)\sin 4\theta/\rho^4\Big] + \frac{\rho^2\left(\rho^2 - m\cos 2\theta\right)}{\rho^4 + m^2 - 2m\rho^2\cos 2\theta}\Re \\
& \cdot\left[\left[R^2 B_2'\rho^3/3 + \left[R^2\left[4B_2\left(1+3m^2\right)/3 + 2mB_2'\right] + B_0'\right]/\rho^3\right]\sin 3\theta\right. \\
& \left. + \left[\left(B_0' + 2mR^2 B_2'/3\right)\rho + 2\left[\left(1+m^2\right)\left(b_o + 2mR^2 B_2\right) + m\left(B_0' + mR^2 B_2'\right)\right]/\rho\right]\sin\theta\right. \\
& \left. + R^2\left(8mB_2/3 + B_2'\right)\sin 5\theta/\rho^5\right] - \rho\left[\left[\rho^4\left(1-m\right) - \rho^2 + m\right]\cos\theta - m^2\left(1-\rho^2\right)\cos 3\theta\right] \\
& /\left(\rho^4 + m^2 - 2m\rho^2\cos 2\theta\right)\cdot\sum_{n=1}^{\infty} R^{4n}\left[\Re B_{4n}\left(\Im\frac{dG_{4n}^{0}}{d\zeta} - \frac{1}{4n+1}\Im\frac{dG_{4n+1}^{\infty}}{d\zeta}\right) + \frac{\Re B_{4n}'}{4n+1}\Im\frac{dG_{4n+1}^{0}}{d\zeta}\right. \\
& \left. + R^2\left(\Re B_{2(2n+1)}\left(\Im\frac{dG_{2(2n+1)}^{0}}{d\zeta} - \frac{1}{4n+3}\Im\frac{dG_{4n+3}^{\infty}}{d\zeta}\right) + \frac{\Re B_{2(2n+1)}'}{4n+3}\Im\frac{dG_{4n+3}^{0}}{d\zeta}\right)\right] \\
& + \sum_{n=1}^{\infty} R^{4n}\left[\Re B_{4n}\left(\frac{\Im G_{4n+1}^{0}}{4n+1} - \Im G_{4n}^{\infty}\right) - \frac{\Re B_{4n}'\Im G_{4n+1}^{\infty}}{4n+1}\right. \\
& \left. + R^2\left(\Re B_{2(2n+1)}\left(\frac{\Im G_{4n+3}^{0}}{4n+3} - \Im G_{2(2n+1)}^{\infty}\right) - \frac{\Re B_{2(2n+1)}'\Im G_{4n+3}^{\infty}}{4n+3}\right)\right] \\
& - \frac{\rho\left(\rho^4\sin\theta + m^2\sin 3\theta\right)}{\rho^4 + m^2 - 2m\rho^2\cos 2\theta}\Re\left[b_o + mR^2 B_2\right. \\
& \left. + \left[R^2 B_2\rho^2 + \left[mb_o + B_0' + R^2\left[\left(1+2m^2\right)B_2 + mB_2'\right]\right]/\rho^2\right]\cos 2\theta + R^2\left(3mB_2 + B_2'\right)\cos 4\theta/\rho^4\right] \\
& - \frac{m\rho^2\sin 2\theta}{\rho^4 + m^2 - 2m\rho^2\cos 2\theta}\Re\left[\left[R^2 B_2'\rho^3/3 - \left[R^2\left[4B_2\left(1+3m^2\right)/3 + 2mB_2'\right] + B_0'\right]/\rho^3\right]\cos 3\theta\right. \\
& \left. + \left[\left(B_0' + 2mR^2 B_2'/3\right)\rho - 2\left[\left(1+m^2\right)\left(b_o + 2mR^2 B_2\right) + m\left(B_0' + mR^2 B_2'\right)\right]/\rho\right]\cos\theta\right. \\
& \left. - R^2\left(8mB_2/3 + B_2'\right)\cos 5\theta/\rho^5\right] \\
& - \rho\left[\left[\rho^4\left(1+m\right) - \rho^2 - m\right]\sin\theta + m^2\left(1-\rho^2\right)\sin 3\theta\right]/\left(\rho^4 + m^2 - 2m\rho^2\cos 2\theta\right) \\
& \cdot\sum_{n=1}^{\infty} R^{4n}\left[\Re B_{4n}\left(\frac{1}{4n+1}\Re\frac{dG_{4n+1}^{\infty}}{d\zeta} - \Re\frac{dG_{4n}^{0}}{d\zeta}\right) - \frac{\Re B_{4n}'}{4n+1}\Re\frac{dG_{4n+1}^{0}}{d\zeta}\right. \\
& \left. + R^2\left(\Re B_{2(2n+1)}\left(\frac{1}{4n+3}\Re\frac{dG_{4n+3}^{\infty}}{d\zeta} - \Re\frac{dG_{2(2n+1)}^{0}}{d\zeta}\right) - \frac{\Re B_{2(2n+1)}'}{4n+3}\Re\frac{dG_{4n+3}^{0}}{d\zeta}\right)\right]\Bigg\}.
\end{aligned}
$$

Acknowledgment

The research described in this paper is co-financed by the EU (European Social Fund-ESF) and Greek national funds through the Operational Program "Education and Lifelong Learning" of the National Strategic Reference Framework (NSRF) – Research Funding Program: THALES: Reinforcement of the interdisciplinary and/or inter-institutional research and innovation.

References

1. ISRM, *Suggested methods for determining tensile strength of rock materials*, International Journal of Rock Mechanics and Mining Sciences Abstracts, **15**, 3, 99–103, 1978.
2. ASTM D3967 – 08, *Standard test method for splitting tensile strength of intact rock core specimens*, ASTM Volume **04.08** Soil and Rock (I): D420 D5876, 2014.
3. ISRM, (Coordinator Fowell R.J.), *Suggested methods for determining mode-I fracture toughness using CCNBD specimens*, International Journal of Rock Mechanics and Mining Sciences, **32**, 1, 57–64, 1995.
4. Wang Q.Z., Fan H., Gou X.P., Zhang S., *Recalibration and clarification of the formula applied to the ISRM-suggested CCNBD specimens for testing rock fracture toughness*, Rock Mechanics and Rock Engineering, **46**, 303–313, 2013.
5. Kourkoulis S.K., Markides Ch.F., *Fracture toughness determined by the centrally cracked Brazilian disc test: Some critical issues in the light of an alternative analytic solution*, ASTM Materials Performance & Characterization, **3**, 3, 45–86, 2014.
6. Markides Ch.F., Kourkoulis S.K., *Naturally accepted boundary conditions for the Brazilian disc test and the corresponding stress field*, Rock Mechanics and Rock Engineering, **46**, 5, 959–980, 2013.
7. Burniston E.E., *An example of a partially closed Griffith crack*, International Journal of Rock Mechanics and Mining Sciences, **5**, 17–24, 1969.
8. Tweed J., *The determination of the stress intensity factor of a partially closed Griffith crack*, International Journal of Engineering Science, 793–803, 1970.
9. Pazis D.N., Theocaris P.S., Konstantellos B.D., *Elastic overlapping of the crack flanks under mixed-mode loading*, International Journal of Fracture, **37**, 303–319, 1988.
10. Markides Ch.F., Pazis D.N., Kourkoulis S.K., *The centrally cracked Brazilian disc: Closed solutions for stresses and displacements for cracks under opening mode*, Journal of Engineering Mathematics, **83**, 1, 143–168, 2013.
11. Markides Ch.F., Pazis D.N, Kourkoulis S.K., *The centrally cracked Brazilian disc: Implications and solutions in case of closing cracks*, Journal of the Mechanical Behaviour of Materials, **23**, 3–4, 59–77, 2014.
12. Atkinson C., Smelser R.E., Sanchez J., *Combined mode fracture via the cracked Brazilian disk test*, International Journal of Fracture, **18**, 279–291, 1982.
13. Markides Ch.F., Pazis D.N., Kourkoulis S.K., *Stress intensity factors for the Brazilian disc with a short central crack: Opening versus closing cracks*, Applied Mathematical Modelling, **35**, 12, 5636–5651, 2011.

14. Theocaris P.S., Sakellariou M., *A correction model for the incompatible deformations of the shear internal crack*, Engineering Fracture Mechanics, **38**, 231–240, 1991.

15. Kourkoulis S.K., Markides Ch.F., Chatzistergos P.E., *The standardized Brazilian disc test as a contact problem*, International Journal of Rock Mechanics and Mining Sciences, **57**, 132–141, 2012.

16. Markides Ch.F., Kourkoulis S.K., *The stress field in a standardized Brazilian disc: The influence of the loading type acting on the actual contact length*, Rock Mechanics and Rock Engineering, **45**, 2, 145–158, 2012.

17. Kolosov G.V., *Application of the Complex Variable to the Theory of Elasticity* (in Russian), ONT1, Moscow-Leningrad, 1935.

18. Muskhelishvili N.I., *Some Basic Problems of the Mathematical Theory of Elasticity*, Noordhoff, Groningen, The Netherlands, 1963.

19. Kourkoulis S.K., Markides Ch.F., Pasiou E.D., *A combined analytic and experimental study of the displacement field in a circular ring*, Meccanica, DOI 10.1007/s11012-013-9846-0, Published on line 06 December 2013.

20. Markides C.F., Pazis D.N., Kourkoulis S.K., *Closed full-field solutions for stresses and displacements in the Brazilian disk under distributed radial load*, International Journal of Rock Mechanics and Mining Sciences, **47**, 2, 227–237, 2010.

21. Kourkoulis S.K., Markides Ch.F., Chatzistergos P.E., *The Brazilian Disc under parabolically varying load: Theoretical and experimental study of the displacement field*, International Journal of Solids and Structures, **49**, 7–8, 959–972, 2012.

22. Hondros G., *The Evaluation of Poisson's Ratio and the Modulus of Materials of a low Tensile Resistance by the Brazilian (Indirect Tensile) Test with Particular Reference to Concrete*, Australian Journal of Applied Science, **10**, 243–268, 1959.

23. Timoshenko S.P., Goodier J.N., *Theory of elasticity* (2nd ed.), McGraw-Hill: Engineering societies monographs, New York, 1951.

Received October 20, 2014; revised version November 3, 2014.